SLAC-PUB-353
September 1967

HIGH-ENERGY PHOTOPRODUCTION*

by

B. Richter
Stanford Linear Accelerator Center
Stanford University, Stanford, California

(Paper delivered at the International Symposium on Electron and Photon Interactions at High Energies, SLAC, September 1967)

*Work supported by the U. S. Atomic Energy Commission.

HIGH-ENERGY PHOTOPRODUCTION

B. Richter
Stanford Linear Accelerator Center, Stanford, California

INTRODUCTION

In this paper I shall summarize the most recent experiments on photoproduction reactions leading to two-body final states. Low-energy photoproduction and diffraction processes have been excluded by the organizers of the conference, and in order to reduce the data to manageable proportions and the talk to a finite length, I have introduced a cutoff in the experiments that I will discuss at a photon energy of around 3 GeV. I shall not go below the cutoff too often.

Experimental equipment and methods will be discussed only if details are not available in the published literature.

The paper is organized as follows:

I. π^+ photoproduction

II. π^0 photoproduction

III. $K^+\Lambda$ and $K^+\Sigma$ photoproduction

IV. Miscellaneous experiments

I. π^+ PHOTOPRODUCTION

A. Experiments

1. The first of the new experiments that I shall discuss was done at the Stanford Linear Accelerator Center by a group composed of A. Boyarski, F. Bulos, W. Busza, R. Diebold, S. Ecklund, G. Fischer, J. Rees, and B. Richter.[1] The experiment covered a region of photon energies from 5 to 16 GeV and a range of momentum transfers from 2×10^{-4} to $2(\mathrm{GeV/c})^2$. The SLAC 20-GeV/c spectrometer was used for detection.

Figure 1 is a schematic of the spectrometer. The magnets bend particles in the vertical plane. Particles that leave the target with different angles in the vertical plane are brought to a first focus at the center of the spectrometer, and then brought to a second focus in the detector housing. A hodoscope at the second focus measures the displacement of the image from the center line of the system, and hence determines the momentum. In the horizontal plane, parallel rays are brought to a focus in the detector housing where a second hodoscope measures the horizontal image displacement and thereby determines the horizontal angle relative to the axis of the system. The magnet system is corrected for chromatic aberrations by 3 sextupole magnets and the inherent resolution of the whole system is about 0.1% in momentum and 0.3 milliradian in angle. The acceptance of the system is ± 4 milliradians in angle, $\pm 1.8\%$ in momentum, and 1.2×10^{-4} steradians in solid angle.

A schematic of the detection systems is shown in Fig. 2. In addition to the indicated momentum (P) and angle (θ) hodoscopes, two other hodoscopes are used (X and ϕ). Information from the P and ϕ hodoscopes is used to determine a particle's momentum and angle in the vertical plane. The vertical angle is determined to a resolution of 1.5 millirad. Information from the X and θ hodoscopes is used to determine the horizontal production angle and to reject particles which have come from the magnet poles.

Particles are identified by use of a differential Cerenkov counter, a shower counter, and a muon range telescope. The differential Cerenkov counter is the coincidence-anticoincidence type, and is used to identify protons, K-mesons, or the group of pion, muon, and electron. Electrons are identified by pulse height in the shower counter, and muons by range in iron absorber.

In operation, a coincidence between the three trigger counters ($T_1T_2T_3$) generates a fast gate whose presence allows passage of hodoscope and range counter information, and pulse-height information from both the inner and outer rings of the Cerenkov counter and from the shower counter to an SDS 9300 computer which is used on-line in the experiment. A criterion on range in the iron and pulse height in the shower counter is used to isolate the strongly-interacting particle, and the differential Cerenkov counter pulse heights are used to separate members of the strongly-interacting group into p, K, or π.

In order to determine the yield of a particular reaction, the spectrometer momentum was set to correspond to that of particles produced by photons of the maximum energy in the photon beam. The hodoscope information was used to compute the distribution in missing mass of all the events assuming that the photon energy was equal to the bremsstrahlung maximum. If one assumes that the cross section does not vary significantly over the few-percent momentum acceptance of the spectrometer, the missing mass distribution has the same shape as the bremsstrahlung spectrum folded with the overall resolution of the system. The missing mass distribution was therefore fitted with a step function suitably smeared out at the beginning of the step to approximate closely the energy distribution of the photons near the tip of the bremsstrahlung distribution, plus a polynomial in the missing mass which begins at the threshold for production of three-body final states.

Figure 3 shows the data and a fitted curve for π^+ production, while Fig. 4 shows the data and fitted curve for K^+ production.

2. An experiment on π^+ production has been done recently at CEA by a group composed of P. M. Joseph, N. Hicks, L. Litt, F. M. Pipkin, and J. J. Russell.[2] They covered a few momentum transfers between 0.1 and 1.5 $(\mathrm{GeV}/c)^2$ for photon energies of 3.4 and 5 GeV.

The spectrometer and detection system used was basically the same as has been previously used by the Pipkin group and will therefore not be described here.

As in the experiment described previously, the momentum variation of the pion yield was measured in order to isolate the single-pion production channel. Figure 5 shows the procedure for a typical point. The pion momentum spectrum was fitted with the assumed shape of the single pion yield, plus a curve to account for the decay of photoproduced ρ mesons, plus an inelastic background whose shape is based on a formula by Drell.[3]

3. An experiment on π^+ production near zero degrees has just been completed at DESY by Buschhorn et al.[4] They have preliminary results on the cross section for photons of 2.7 and 4.9 GeV at momentum transfers between 10^{-4} $(\mathrm{GeV/c})^2$ and 2×10^{-3} $(\mathrm{GeV/c})^2$. The experiment was done with their spectrometer, and the equipment and procedures are similar to those described by the group in previous publications.

B. Results and Interpretations

Figure 6 shows the results of the SLAC high-energy forward-production experiment of Boyarski et al. and the 5 GeV data of Joseph et al. The data show two striking features — a sharp rise in the cross section at very small momentum transfers, and very similar shapes at all momentum transfers.

Figure 7 shows the small-momentum-transfer region in more detail. The new DESY small-angle data are included. $S(d\sigma/d\Omega)_{c.m.}$, where S is the square of the total energy in the center-of-mass system, is plotted versus the square of the 4-momentum transfer t. The data show that there is no sign of a forward dip in the cross section down to very small momentum transfers, and that S times the small-momentum-transfer center-of-mass differential cross section is nearly independent of energy. The earlier experiment of Buschhorn et al.[5] at energies up to 3 GeV has shown this same type of behavior of the forward cross section. There has been a tendency to regard this peaking of the forward cross section shown in the lower-energy experiment as being due to effects of various π-N resonances. The behavior of the high-energy cross section makes this explanation untenable.

The forward cross section can be understood in terms of the Born approximation. Figure 8 shows two Feynman diagrams for π^+ production. Diagram (a) is not by itself gauge invariant, and to maintain gauge invariance one must include an S-channel contribution from the nucleon current. The amplitude is given by[6]

$$A \propto \bar{u}(p')\, \gamma_5 \left\{ \frac{\epsilon \cdot q}{k \cdot q} - \frac{\epsilon \cdot p}{k \cdot p} - \frac{i\sigma_{\mu\nu}}{2k \cdot p}\, \epsilon^{\mu} k^{\nu} \right\} u(p) \quad , \tag{1}$$

where the first term inside the bracket comes from diagram (a) and the other two terms come from diagram (b). The minimal gauge-invariant form given by

$$A_m \propto \left\{ \frac{\epsilon \cdot q}{k \cdot q} - \frac{\epsilon \cdot p}{k \cdot p} \right\} \tag{2}$$

does vanish at 0°, but the remaining term which has the same energy dependence as A_m does not. If the amplitude given by Eq. (1) is used, the cross section is given by

$$S \frac{d\sigma}{d\Omega}_{c.m.} \approx 20.7 \frac{1 + (t^2/m_{\pi}^4)}{\left[1 - (t/m_{\pi}^2)\right]^2} \quad \text{microbarn (GeV)}^2/\text{steradian}, \qquad (3)$$

where the π-N coupling constant has been assumed to be $g^2/4\pi = 14.7$.

Figure 9 shows the zero-degree cross section from several experiments versus photon energy. The 0° cross section from Ecklund and Walker[7] is obtained from their fit to the data, and the other points have been extrapolated to 0° by using Eq. (3). The line is the value predicted by Eq. (3) with no adjustable constants. It is certainly consistent with the high-energy data.

The $\sigma_{\mu\nu}$ term in the amplitude (1) contributes only to low partial waves ($j = 1/2$). Since absorption effects are expected to play an important part in high-energy processes, one can ask: What happens to the forward cross section if the low partial waves are absorbed out? If the absorption is done on the entire amplitude (1) and not merely by removing the $\sigma_{\mu\nu}$ term, the forward cross section is nearly unchanged. The absorption of the $j = 1/2$ partial waves eliminates the $\sigma_{\mu\nu}$ term and changes the value of 0° cross section given by the minimal gauge-invariant form, Eq. (2), to a value close to that given by Eq. (3). Figure 10 shows the results of some calculations by Ecklund[8] on the effect of absorption. $S(d\sigma/d\Omega)_{c.m.}$ is plotted versus the incident photon energy for total absorption of all partial waves with $j \leq J_M$. It is clear that the zero-degree cross section at high energies is quite insensitive to the value of J_M.

We now return to the data at momentum transfers up to 2 $(\text{GeV}/c)^2$. Figure 6 shows that the 8 to 16 GeV data appears to have a break in its slope at a momentum transfer of 0.5 to 0.6 $(\text{GeV}/c)^2$. The t dependences are

$$\frac{d\sigma}{dt} \propto e^{3.1t} \qquad (-t > 0.6)$$

$$\frac{d\sigma}{dt} \propto e^{2t} \qquad (-t < 0.5)$$

Regge exchange models predict a cross section of the form[9]

$$S^2 (d\sigma/dt) \propto F(t)\, S^{2\alpha(t)} , \qquad (4)$$

where F(t) is a function of momentum transfer, and $\alpha(t)$ is the value of the trajectory at the momentum transfer t. Figure 11 shows α, computed from the S-dependence of the cross section at fixed t, versus t. In order to avoid an old problem that has plagued electron machines in the past, that of relative normalizations between laboratories, I have plotted separately α as determined from the SLAC data[1] and as given in the CEA paper.[2]

The behavior of α as shown in Fig. 11 is not consistent with a simple Regge-ized one-pion exchange model, because the π-trajectory passes through zero at $t = +0.02$ $(\mathrm{GeV/c})^2$, and should reach between -1/2 and -1 at -t of 1 $(\mathrm{GeV/c})^2$. I think it will be difficult to fix the simple Regge exchange model by the addition of a few more trajectories since the candidates that I know of have trajectories which pass through zero at $-t \leq 0.5$ $(\mathrm{GeV/c})^2$, and the data show that α remains near zero to considerably larger momentum transfers. However, it is probably true that the Regge exchange model is young enough and flexible enough to accommodate these data at the cost of making the theory more complicated.

I have just received preliminary results from the Ritson group[10] at Stanford on backward π^+ photoproduction. Their data cover the region of u (square of the momentum transfer in the crossed channel) from 0 to -0.6 $(\mathrm{GeV/c})^2$ and photon energies from a few to 10 GeV. The results are shown in Fig. 12. The data show a smoothly varying cross section that becomes more strongly peaked at 180° as the photon energy increases.

I have extrapolated the preliminary data to $u = 0$ and find an S-dependence of cross given by

$$S^2 (d\sigma/du) \propto S^{0.15 \pm 0.35} \ \mu\mathrm{barn}\ (\mathrm{GeV})^2 \tag{5}$$

for photon energies of from 4.3 to 9.8 GeV. The magnitude of this cross section is about 100 times smaller than the forward cross sections of SLAC and DESY. From this one can tentatively conclude that S-channel effects do not play an important role in the forward photoproduction since S-channel terms would give a large cross section for both forward and backward production. Absorption of low partial waves, which eliminates the S-channel terms, must therefore play an important role in photoproduction.

The backward π^+ photoproduction data can also be compared to the backward π-p elastic scattering. Figure 13 shows the π-p elastic data from the paper by Orear et al.[11] The π^+-p elastic data seem to show a dip at $u = -0.2$, to have a much steeper rise than the π^--p data as the scattering angle goes to 180°, and to be about 5 times larger than the π^-p cross section at 180°. The difference between the π^+-p and π^--p data is usually explained in terms of the allowed baryon exchanges.[11] π^--p can go only through N^{*++} exchange, while π^+-p can go through N* and nucleon exchange. Since the π^+ backward photoproduction can also go through both N* and nucleon exchange, one might naively expect that the backward photoproduction would look something like the π^+ elastic scattering. It clearly does not, but the significance of the difference is not clear since as far as I know, no one has calculated what to expect in the photoproduction process including all the spinology.

II. π^0 PHOTOPRODUCTION

A. Experiments

1. A group from Bonn, consisting of M. Braunschweig, W. Braunschweig, D. Husman, K. Lübelsmeyer, and D. Schmitz,[12] has measured the small-angle π^0 production cross section at energies of 4 to 5.8 GeV. The work was done at the DESY synchrotron using a slightly modified version of apparatus which has been described in previous publications.[13]

2. The Osborne group at MIT has recently published the results of work done at CEA covering the large-momentum-transfer region for photon energies of up to 6 GeV.[14]

3. The DESY group of Buschhorn et al., has contributed the results of a recent experiment on the photoproduction of π^0 mesons at 180°.[15] They used the same spectrometer with which the group has done its π^+ production experiments, and detected the recoil protons at 0° in the laboratory. The proton momentum in the range of energies covered is 300 - 400 MeV/c higher than the photon energy, allowing the very high background of pairs from the target to be rejected by slits in the spectrometer.

B. Results and Interpretation

Figure 14 shows the differential cross section $d\sigma/dt$ versus momentum transfer obtained in the Bonn experiment, together with the results of a previous experiment by this group at a lower energy. Some of the points from CEA experiments have been included. Note particularly the behavior of the cross section near zero momentum transfer. At 2.0 and 3.0 GeV the cross section has a sharp dip near $t = 0$. At 4 GeV it looks flat, and at 5 and 5.8 GeV it shows a sharp rise. The Bonn group explains this as being due to the Primakoff effect,[16] i.e., π^0 production by the interaction of the photon with the coulomb field of the proton. Production by this mechanism, which is the inverse of the π^0 decay, is very sharply peaked in the forward direction and increases rapidly with incident energy.

The curves are the result of a fit of the data model by Ader et al.,[17] which includes Regge-ized ω and B meson exchange. The trajectories used were

$$\alpha_\omega(t) = 0.45 + 0.9\,t$$

$$\alpha_B(t) = -0.32 + 0.9\,t \quad .$$

A three-parameter fit was made by adjusting the ω and B couplings in the helicity amplitudes. The fit is not good at 2 and 3 GeV, which is not surprising since some resonant contribution to the cross section is expected at these low energies, but reproduces the general features of the data fairly well at the higher energies.

Figure 15 shows the Bonn data at 5.8 GeV and small momentum transfer on an expanded scale. The triangles are the calculated values for the Primakoff effect with constructive or destructive interference with the Regge-ized ω and B exchange; the π^0 lifetime used was $0.74 \pm 0.1 \times 10^{-16}$ sec, as measured by Belletini et al.[18] The agreement with experiment for constructive interference is quite good.

Figure 16 shows the latest CEA data from 2 to 5 GeV; $d\sigma/dt$ *versus* momentum transfer for constant photon energy, and $d\sigma/dt$ *versus* photon energy for constant momentum transfer. The data extend to momentum transfers much larger than those obtained in the Bonn experiment and show a flat region in cross section for approximately $0.5 < -t < 1.5$ $(GeV/c)^2$, followed by a decrease and then, at the lower energies, a rise in the backward direction. The straight lines on the plot of $d\sigma/dt$ *versus* photon energy are used to derive the momentum-transfer dependence of the ω Regge trajectory in a model containing only Regge-ized ω exchange. They find a trajectory given by

$$\alpha_\omega(t) = (0.47 \pm 0.03) + (0.85 \pm 0.05)\, t \quad .$$

However, I think that because of the large momentum transfers and relatively low photon energies, this fit may push a simple model much too far. At angles around 90° in the center-of-mass system, u-channel exchange could be as important as t-channel exchange, and at $-t$ of 3 and 4 $(GeV/c)^2$, all of the points with good statistics, which actually determine the value of α, have center-of-mass angles of greater than 90°.

In Fig. 17, I have plotted $S^2(d\sigma/dt)$ *versus* momentum transfer for the Bonn π^0 data. Regge-ized particle exchange gives a cross section of the form

$$S^2(d\sigma/dt) = f(t)\, S^{2\alpha} \quad ,$$

where $f(t)$ is a function of momentum transfer, and α is the trajectory of the exchanged particle. Models such as that of Ader *et al.*, which include the effects of more than one particle exchange, have a sum of such terms with each term representing the effect of a different particle. It is clear that no S dependence of $S^2(d\sigma/dt)$ is required to fit the data. However, the errors on the points are large, and the range of S is small, and the data are not inconsistent with Regge-ized exchange models. More data are needed in this momentum-transfer range for much higher incident photon energies. Until such data are available, one cannot make firm conclusions about the applicability of Regge-pole models to π^0 photoproduction.

The last π^0 data to be discussed is the 180° cross section measured by Buschhorn *et al.*, [19] and illustrated in Fig. 18. The peaks and valleys in the cross section seem to correspond to the positions of the known π-N resonances. Some of the structural features appear to be shifted by about 100 MeV in photon energy with respect to the resonances, but this can easily occur when broad peaks are superposed on a steeply varying background. I have compared these data with the π^--p backward elastic-scattering data, [20] and find that the only significant differences between the two results are that the π-p cross section is larger than the γ-p by a factor 137π, and the dip in the region of the N* (2190) is considerably deeper in the π-p scattering experiment.

III. K^+ PHOTOPRODUCTION

The SLAC group of Boyarski et al., has also done extensive measurements on $K^+\Lambda^0$ and $K^+\Sigma^0$ photoproduction. The range of momentum transfers and photon energies is the same as for the π^+ photoproduction data discussed above.

The K-Λ data are shown in Fig. 19. The small-angle K^+ data are quite different from the π^+ data in that the K-Λ cross section has a distinct dip near zero degrees rather than the rise shown by the π^+ cross section. At small momentum transfers the S-dependence of the cross section is such that $d\sigma/dt$ decreases with S more rapidly than S^{-2} between 5 and 8 GeV and decreases about as S^{-2} thereafter. The same effect was shown in the π^+ data.

The t-dependence of the points with momentum transfer greater than about $-0.5\ (\mathrm{GeV/c})^2$ are well fitted by an exponential with the same slope as was used to fit the π^+ data ($e^{3.1t}$).

Figure 20 shows the ratio of $K^+\Sigma^0$ to $K^+\Lambda^0$ cross sections. The errors in the determination of K-Σ cross section are considerably larger than for the K-Λ cross section, but the data show that the Σ^0/Λ^0 cross section ratio is about unity for $-t \geq 0.2\ (\mathrm{GeV/c})^2$. The measurement of Elings et al.,[21] at CEA also shows a Σ/Λ ratio of around 1 for a photon energy of 3.4 GeV.

At small momentum transfers, the Σ/Λ ratio seems to decrease. This is shown clearly in the 5- and 8-GeV data; the 11- and 16-GeV data are consistent with the two lower energies, but the accuracy of the experiment is not sufficient to draw quantitative conclusions, and the Σ/Λ ratio could remain about 1 down to much smaller momentum transfers.

The K-Λ, K-Σ and π-N cross sections can be used to test SU_3 symmetry. Unbroken SU_3 symmetry predicts a relation between the photoproduction amplitude given by[22]

$$\sqrt{2}\,A(\pi^+N) = -\sqrt{3}\,A(K^+\Lambda^0) - A(K^+\Sigma^0) \tag{6}$$

With only cross-section data available, this can be written as

$$2\sigma(\pi^+N) = \left| \left[3\sigma(K^+\Lambda)\right]^{1/2} + \left[\sigma(K\Sigma)\right]^{1/2} e^{i\phi} \right|^2 \quad , \tag{7}$$

where the introduction of the phase angle ϕ reflects our lack of knowledge of the relative phase of the $K\Lambda$ and $K\Sigma$ amplitudes. SU_3 symmetry is not violated if $|\cos\phi| \leq 1$.

Figure 21 shows $\cos\phi$ versus t as calculated from the SLAC data. SU_3 symmetry is violated at momentum transfers of less than $0.1\ (\mathrm{GeV/c})^2$ and is unbroken at larger momentum transfers. The data of Elings et al., at 3.4 GeV for $-t \geq 0.2$ also show SU_3 symmetry to be unbroken in agreement with the SLAC data at higher energies.

Lipkin and Scheck[23] have recently published a prediction of the Σ/Λ ratio obtained by the use of SU(6) wave functions for the baryons. Their prediction gives

$$\sigma(\Sigma)/\sigma(\Lambda) = 1/27 \text{ (pure spin-flip transitions)}$$

$$\sigma(\Sigma)/\sigma(\Lambda) \leq 1/3 \text{ (spin-flip and non-spin-flip)}.$$

Pure spin-flip transitions occur in K^+ photoproduction only for a K angle of zero degrees, and the SLAC data at very small momentum are not sufficiently accurate to give any test of the first prediction. The second prediction, however, can be tested, and it fails for all momentum transfers $-t \geq 0.1$ $(\text{GeV/c})^2$.

Figure 22 shows the Regge trajectory $\alpha(t)$, determined from the S dependence of the $K\Lambda$ cross section for fixed t, versus t. The points have larger errors than for the π^+ data, and give a value of α consistent with zero at least to $-t = 0.5$ $(\text{GeV/c})^2$. This α dependence is inconsistent with simple Regge models involving the exchange of K or K*.

IV. MISCELLANEOUS

1. Bemporad, Braccini, Foa, Lübelsmeyer and Schmitz[24] have measured the η^0 lifetime in an experiment done at DESY. They measured η^0 production via the Primakoff effect and isolated the Primakoff effect from background by measuring the production angular distribution at photon energies of 4.0 and 5.5 GeV from targets of lead, silver, and zinc; and testing for the sharp angular distribution, energy dependence, and Z dependence of the one photon exchange process. They find a partial decay width for $\eta \to \gamma\gamma$ of

$$\Gamma_{\gamma\gamma} = 1.21 \pm 0.26 \text{ keV}$$

2. Finally, I would like to mention an experiment by Bar-Yam *et al.*,[25] done at CEA to study the reactions.

$$\gamma + D \to \pi^- + P + P$$

$$\gamma + D \to \pi^+ + N + N$$

at photon energies around 3 GeV. The data are shown in Fig. 23. Figure 23(a) gives the π^-/π^+ ratio versus t while Fig. 23(c) gives the cross sections as a function of momentum transfer. The π^-/π^+ ratio tends to 0.4 as t decreases. A simple one particle exchange production mechanism would give a π^-/π^+ ratio of one. A possible mechanism for producing a π^-/π^+ ratio different from one would involve the exchange of two particles with different G parity. Measurement of the π^-/π^+ ratio is a sensitive test of opposite G parity exchanges – probably too sensitive for the present sloppy state of the theory. We will need better models to understand the results of this experiment.

REFERENCES

1. A. Boyarski, F. Bulos, W. Busza, R. Diebold, S. Ecklund, G. Fischer, J. Rees, B. Richter; contributed paper.

2. P. M. Joseph, N. Hicks, L. Litt, F. M. Pipkin, J. J. Russell; contributed paper.

3. S. D. Drell, Phys. Rev. Letters 5, 278 (1960).

4. G. Buschhorn, P. Heide, U. Kötz, R.A. Lewis, P. Schmüser, H.J. Skronn; contributed paper.

5. G. Buschhorn, J. Carroll, R. D. Eandi, P. Heide, R. Hübner, W. Kern, U. Kötz, P. Schmüser, H. J. Skronn, Phys. Rev. Letters 18, 571 (1967).

6. S. D. Drell, J. D. Sullivan, Phys. Rev. Letters 19, 268 (1967).

7. S. D. Ecklund, R. L. Walker, Cal. Tech. Preprint CALT-68-110.

8. S. D. Ecklund, private communication.

9. G. Zweig, Nuovo Cimento 32, 659 (1964). G. Kramer, P. Stichel, Z. Physik 178, 519 (1964).

10. R. Anderson, D. Gustavson, G. Jones, J. Johnson, D. Kreinick, R. Prepost, D. Ritson, R. Weinstein; contributed paper.

11. J. Orear, R. Rubenstein, D. B. Searl, D. H. White, A. D. Krisch, W. R. Frisken, A. L. Read, H. Ruderman, Phys. Rev. 152, 1162 (1966).

12. M. Braunschweig, W. Braunschweig, D. Husman, K. Lübelsmeyer, D. Schmitz; contributed paper.

13. M. Braunschweig, D. Husman, K. Lübelsmeyer, D. Schmitz, Phys. Letters 22, 705 (1966).

14. G. C. Bolon, D. Garelick, S. Homma, R. Lewis, W. Lobar, D. Luckey, L. S. Osborne, R. Schwitters, J. Uglum, Phys. Rev. Letters 18, 926 (1967).

15. G. Buschhorn, P. Heide, U. Kötz, R. A. Lewis, P. Schmüser, H. J. Skronn; contributed paper.

16. H. Primakoff, Phys. Rev. 81, 899 (1951).

17. J. P. Ader, M. Capdeville, Ph. Salin; contributed paper.

18. G. Belletini, C. Bemporad, P. L. Braccini, L. Foà, Phys. Letters 18, 333 (1965).

19. G. Buschhorn, P. Heide, U. Kötz, R. A. Lewis, P. Schmüser, H. J. Skronn; contributed paper.

20. S. Kormanyos, A. D. Krisch, J. R. O'Fallon, K. Ruderman, L. G. Ratner, Phys.Rev. Letters 16, 709 (1966).

21. U. B. Elings, K. J. Cohon, D. A. Garelick, S. Homma, R. A. Lewis, P. D. Luckey, L. S. Osborne, Phys. Rev. Letters 16, 474 (1966).

22. C. A. Levinson, H. J. Lipkin, S. Meshkov, Phys. Letters 7, 81 (1963).

23. H. J. Lipkin, F. Scheck, Phys. Rev. Letters 18, 347 (1967).

24. C. Bemporad, P. L. Braccini, L. Foà, K. Lübelsmeyer, D. Schmitz; contributed paper.

25. Z. Bar-Yam, J. de Pagter, M. M. Hoenig, W. Kern, D. Luckey, L. S. Osborne, Phys. Rev. Letters 19, 40 (1967).

FIGURE CAPTIONS

1. Thin lens equivalent of SLAC 20 GeV/c spectrometer.

2. Schematic of the detection system used by the SLAC group for the π^+ and K^+ photoproduction experiments.

3. Typical data from a π^+ run, showing the fit of a π^+ yield and background.

4. Typical data from a K^+ run, showing fit of $K\Lambda$, $K\Sigma$, and background.

5. Typical data and fit from the experiment of Joseph et al.

6. π^+ cross section ($d\sigma/dt$) vs momentum transfer from the experiments of Boyarski et al. and Joseph et al.

7. Small momentum transfer cross section ($S\ d\sigma/d\Omega_{c.m.}$) vs momentum transfer from the experiments of Boyarski et al. and Buschhorn et al.

8. Feynman diagrams for π^+ photoproduction.

9. Extrapolated 0^o cross section ($S\ d\sigma/d\Omega_{c.m.}$) vs photon energy.

10. Effect of absorption on the 0^o π^+ photoproduction cross section, computed in the Born approximation, vs photon energy. The curves show the effect of complete absorption of all partial waves with $j \leq J_M$.

11. Value of Regge trajectory $\alpha(t)$ vs momentum transfer. Points are from the work of Boyarski et al. and Joseph et al. The trajectory has been computed assuming a single exchange.

12. Backward π^+ photoproduction cross section ($d\sigma/du$) vs u, from the work of Anderson et al.

13. π-p backward elastic scattering cross section versus u, from the work of Orear et al. (Reproduced from Ref. 11.)

14. π^o photoproduction cross section vs momentum transfer from the work of Braunschweig et al. The solid lines are the best fit to a Regge model using both ω and B exchange.

15. Small momentum transfer cross section ($d\sigma/dt$) vs t at 5.8 GeV, from the work of Braunschweig et al. The solid line is the cross section computed from the Regge exchange model. The triangles show the cross section calculated by the addition of π^o production via the Primakoff effect for both signs of the interference between the Primakoff effect and the Regge exchange.

16. π^o photoproduction cross sections from the data of Bolon et al. (Reproduced from Ref. 14.).

17. π^o photoproduction cross section (S^2 $d\sigma/dt$) vs momentum transfer, from the experiment of Braunschweig et al.

18. 180^o π^o photoproduction cross section ($d\sigma/d\Omega_{c.m.}$) vs photon energy, from the experiment of Buschhorn et al.

19. $K\Lambda$ photoproduction cross section ($d\sigma/dt$) vs momentum transfer, from the work of Boyarski et al.

20. Ratio $K\Sigma$ to $K\Lambda$ photoproduction cross sections vs momentum transfer, from the experiment of Boyarski et al.

21. Test of SU3 symmetry using the $\pi^+ N$, $K\Lambda$, and $K\Sigma$ data, from the experiment of Boyarski et al. SU3 is unbroken if cos ϕ lies between + 1 and - 1. Cos ϕ is plotted vs momentum transfer.

22. Regge trajectory $\alpha(t)$ for $K\Lambda$ photoproduction, determined from the data of Boyarski et al.

23. π^- and π^+ photoproduction cross sections from deuterium, from the work of Bar-Yam et al. (Reproduced from Ref. 25.)

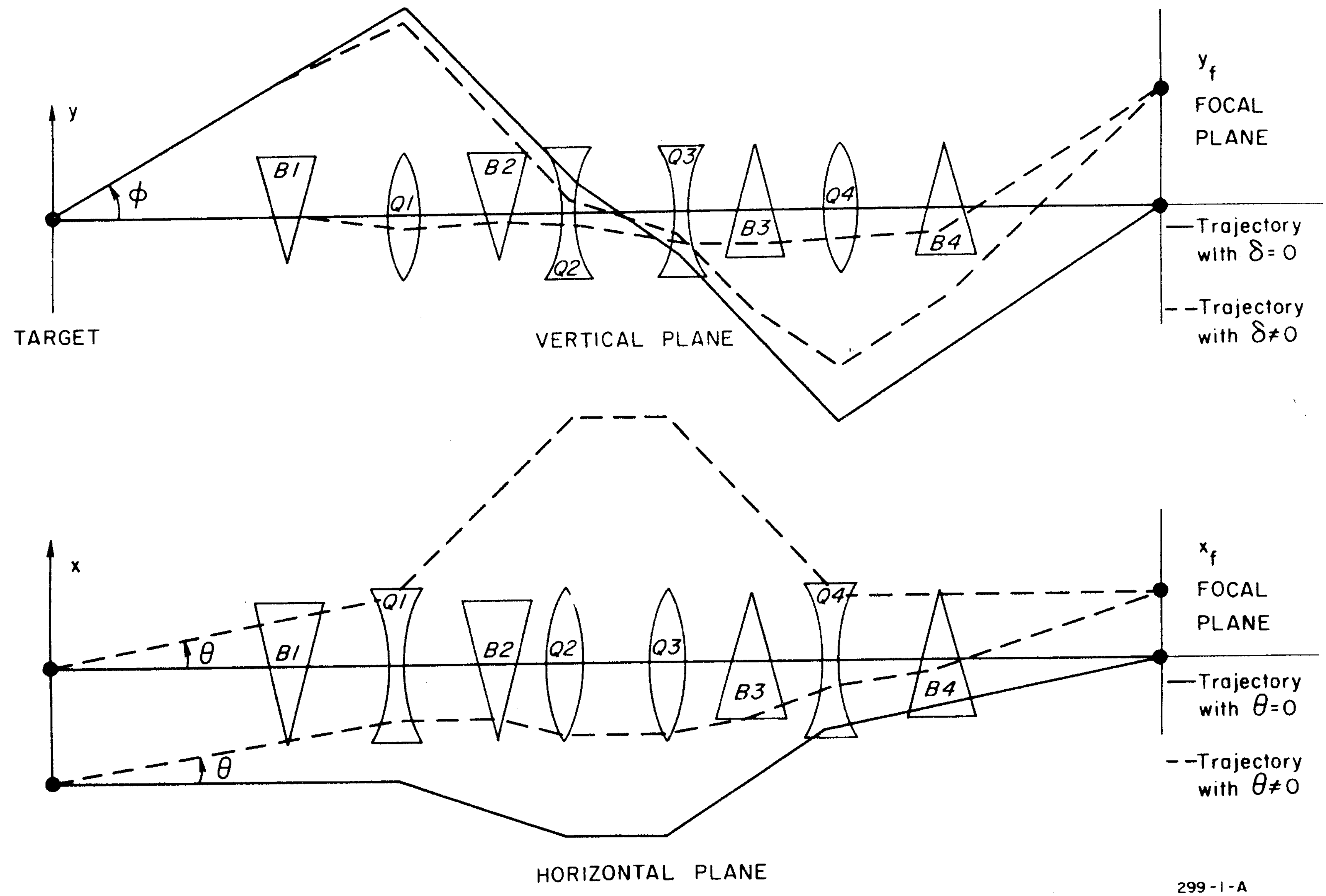

y
φ
TARGET
B1
Q1
B2
Q2
Q3
B3
Q4
B4
y_f
FOCAL
PLANE
—Trajectory
with δ=0
--Trajectory
with δ≠0
VERTICAL PLANE
x
θ
θ
B1
Q1
B2
Q2
Q3
B3
Q4
B4
x_f
FOCAL
PLANE
—Trajectory
with θ=0
--Trajectory
with θ≠0
HORIZONTAL PLANE
299-1-A

FIG. 1

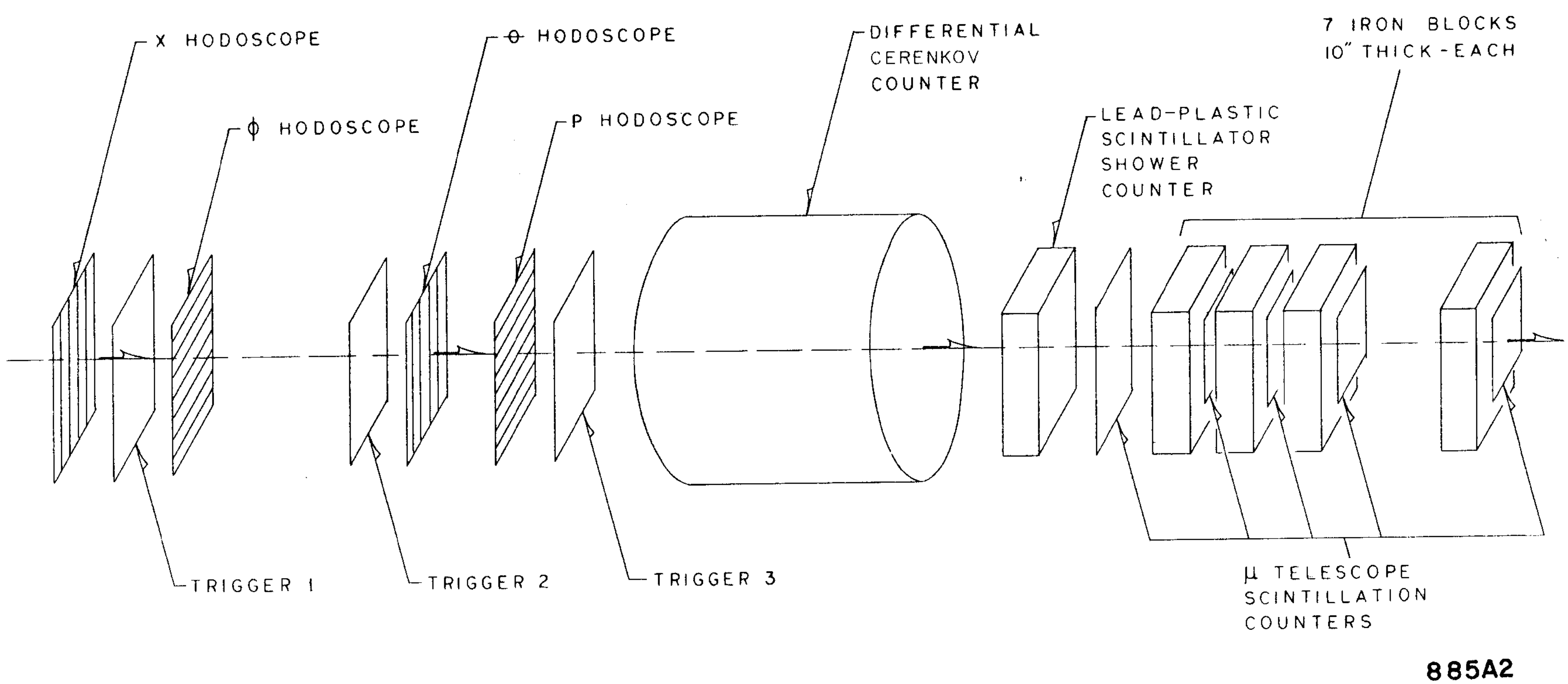
X HODOSCOPE
ϕ HODOSCOPE
θ HODOSCOPE
P HODOSCOPE
DIFFERENTIAL
CERENKOV
COUNTER
LEAD-PLASTIC
SCINTILLATOR
SHOWER
COUNTER
7 IRON BLOCKS
10" THICK-EACH
TRIGGER 1
TRIGGER 2
TRIGGER 3
μ TELESCOPE
SCINTILLATION
COUNTERS
885A2

FIG. 2

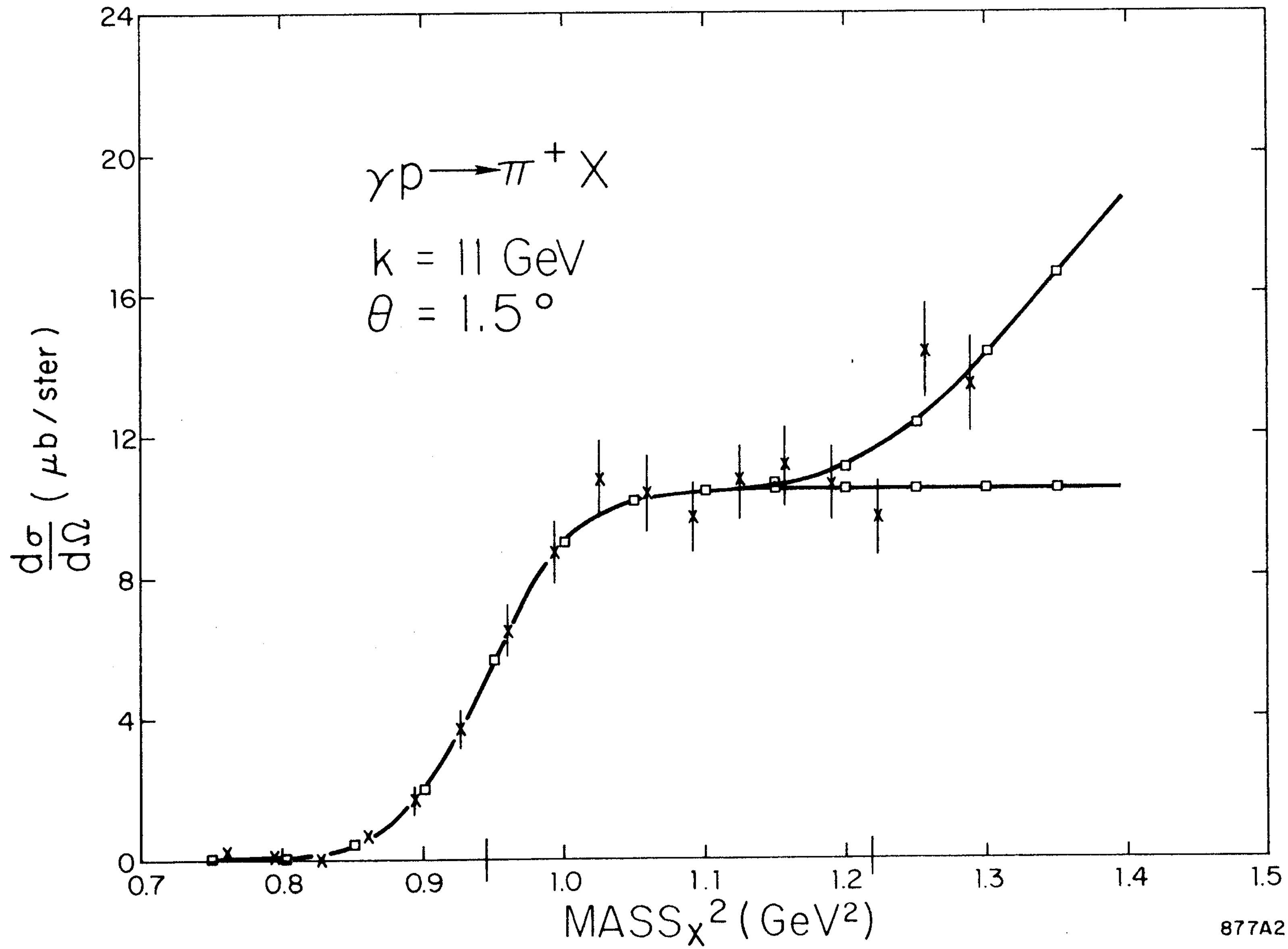

$\gamma p \longrightarrow \pi^+ X$
k = 11 GeV
θ = 1.5°
$\frac{d\sigma}{d\Omega}$ (μb / ster)
0
4
8
12
16
20
24
0.7
0.8
0.9
1.0
1.1
1.2
1.3
1.4
1.5
$\mathrm{MASS}_X{}^2$ (GeV^2)
877A2

FIG. 3

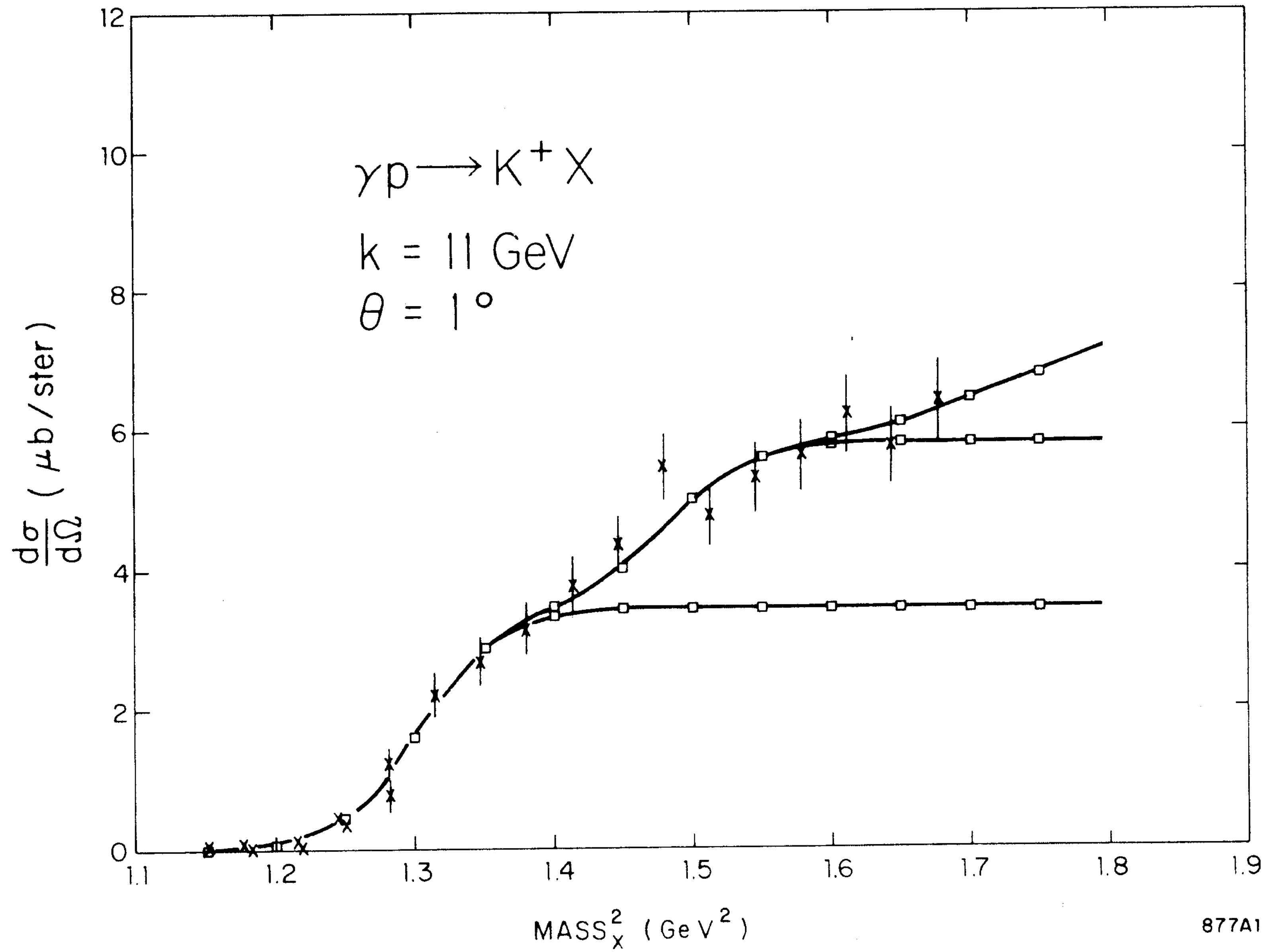

$\gamma p \longrightarrow K^+ X$
k = 11 GeV
$\theta = 1°$
$\frac{d\sigma}{d\Omega}$ (μb / ster)
0
2
4
6
8
10
12
1.1
1.2
1.3
1.4
1.5
1.6
1.7
1.8
1.9
$MASS_X^2$ (GeV^2)
877A1

FIG. 4

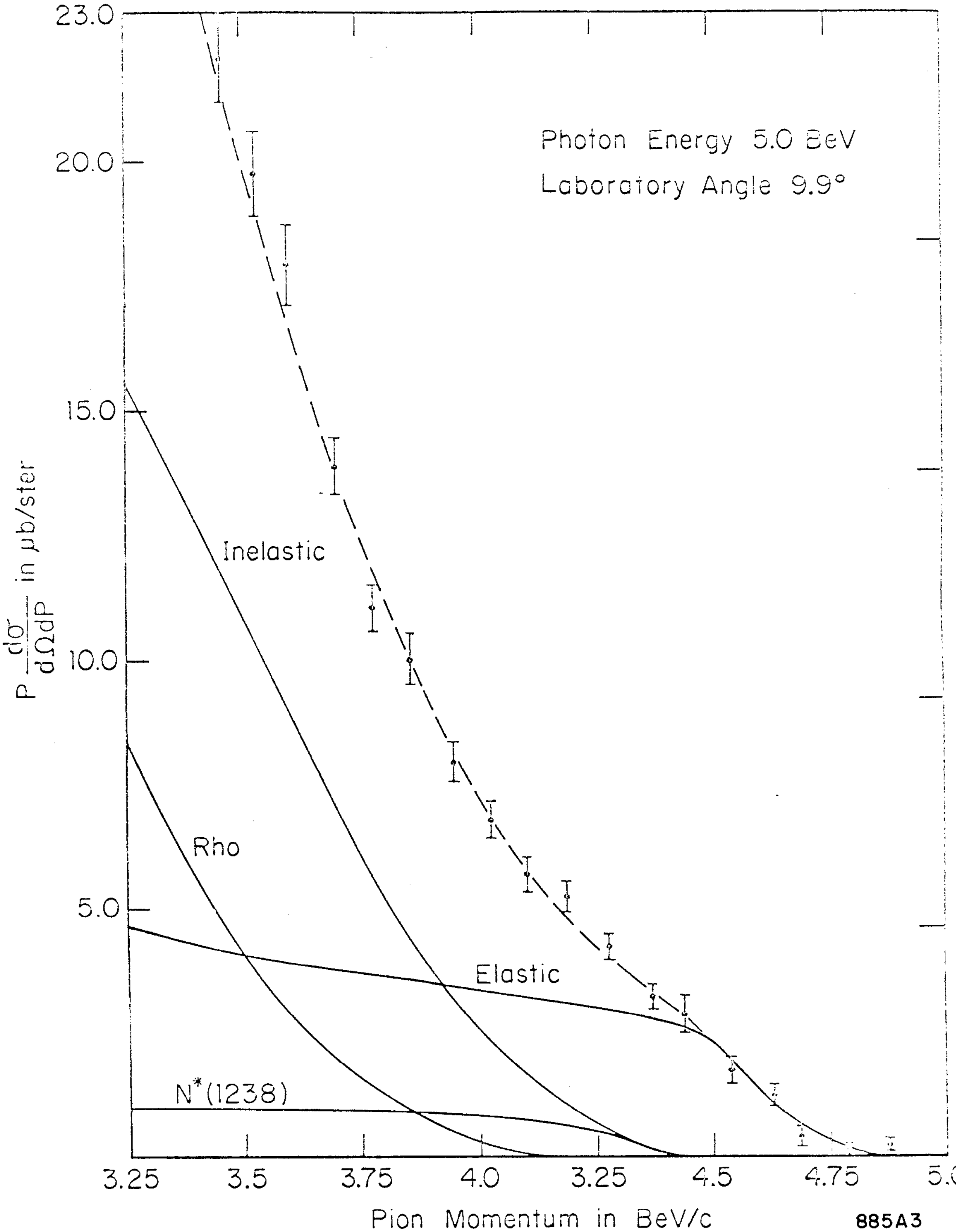
23.0
20.0
15.0
10.0
5.0
Photon Energy 5.0 BeV
Laboratory Angle 9.9°
Inelastic
Rho
Elastic
N*(1238)
$P \frac{d\sigma}{d\Omega dP}$ in μb/ster
3.25
3.5
3.75
4.0
3.25
4.5
4.75
5.0
Pion Momentum in BeV/c
885A3

FIG. 5

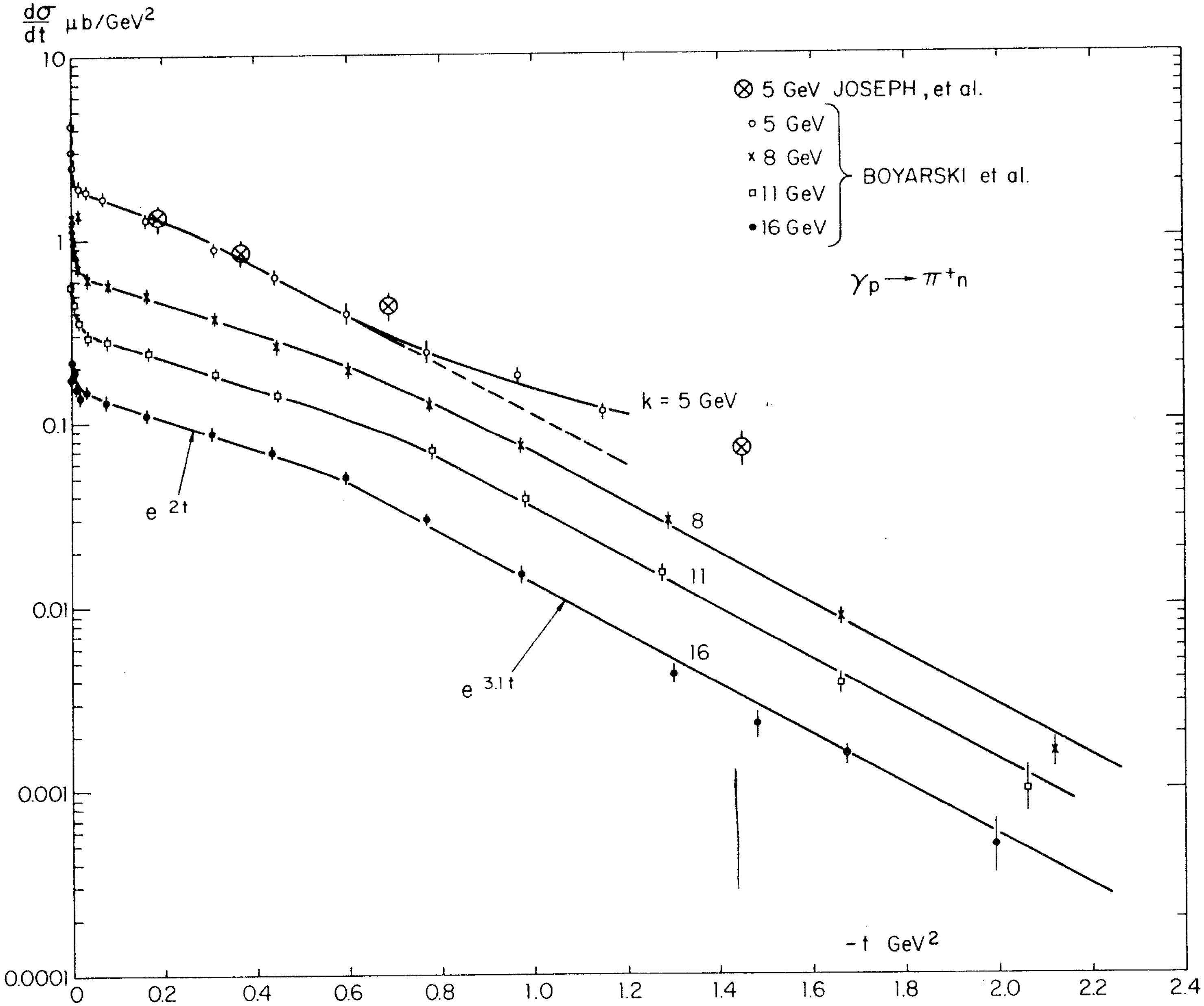
$\frac{d\sigma}{dt}$ μb/GeV^2
10
1
0.1
0.01
0.001
0.0001
0
0.2
0.4
0.6
0.8
1.0
1.2
1.4
1.6
1.8
2.0
2.2
2.4
⊗ 5 GeV JOSEPH, et al.
∘ 5 GeV
× 8 GeV
□ 11 GeV
• 16 GeV
BOYARSKI et al.
$\gamma p \to \pi^+ n$
k = 5 GeV
8
11
16
e^{2t}
$e^{3.1t}$
$-t$ GeV^2

FIG. 6

877C5

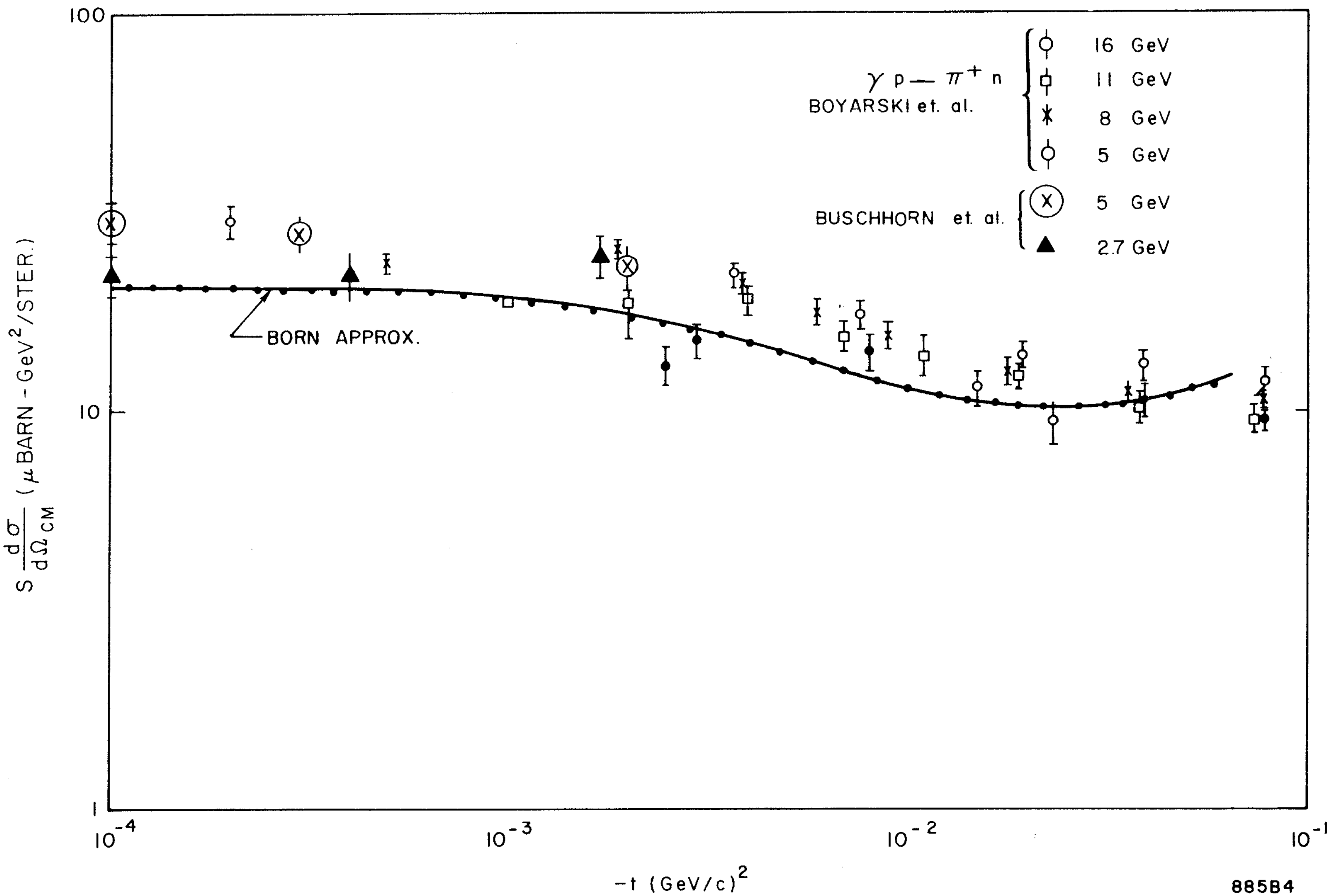

γ p — π⁺ n
BOYARSKI et. al.
16 GeV
11 GeV
8 GeV
5 GeV
BUSCHHORN et. al.
5 GeV
2.7 GeV
BORN APPROX.
100
10
1
10^-4
10^-3
10^-2
10^-1
S dσ/dΩ_CM (μBARN - GeV²/STER.)
−t (GeV/c)²
885B4

FIG. 7

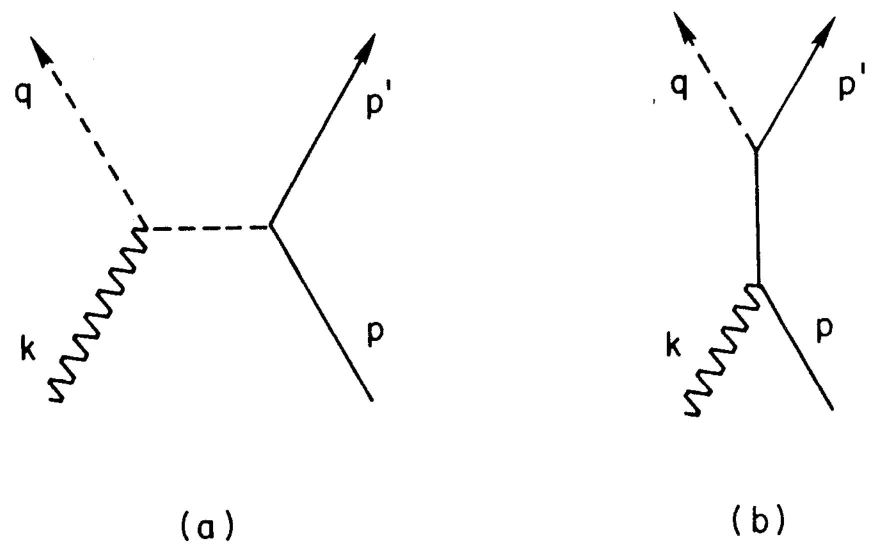

FEYNMAN DIAGRAMS FOR π^+ PHOTOPRODUCTION

885A5

FIG. 8

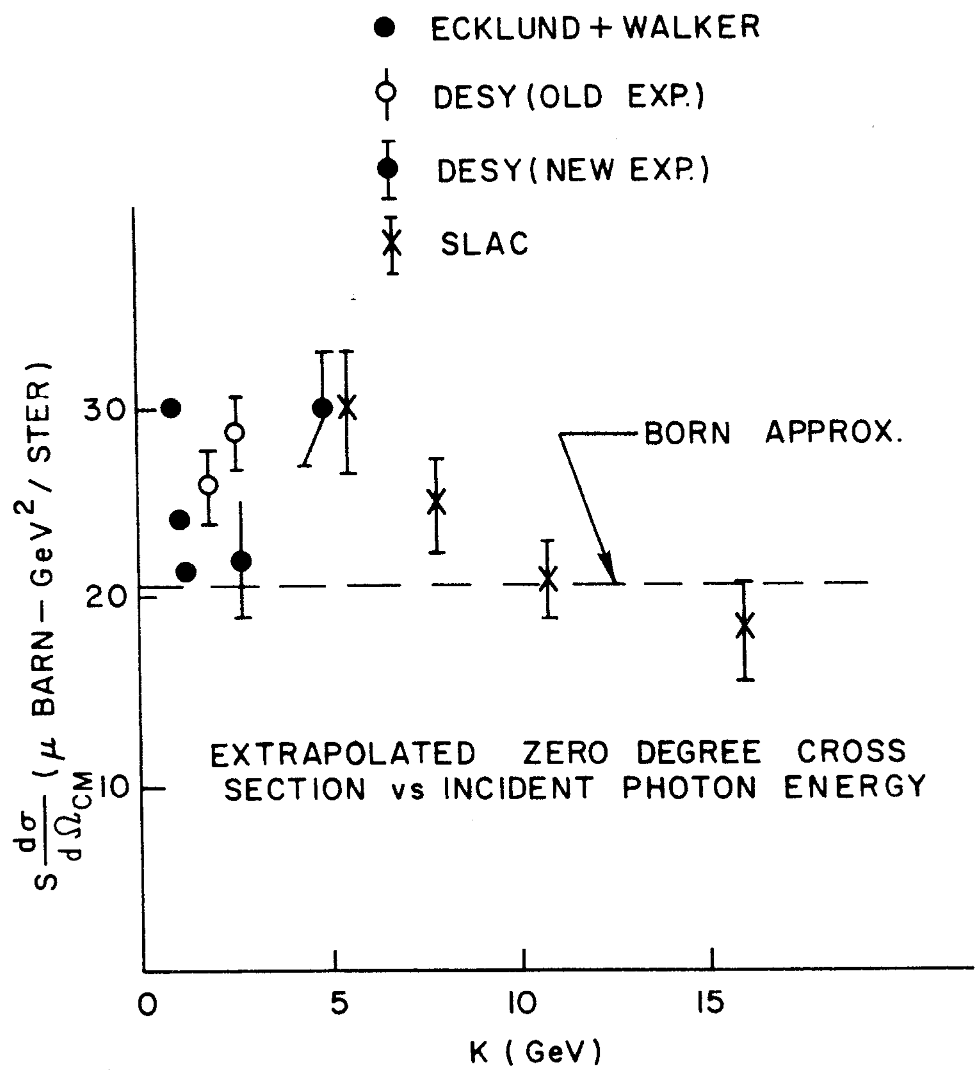

ECKLUND + WALKER
DESY (OLD EXP.)
DESY (NEW EXP.)
SLAC
BORN APPROX.
EXTRAPOLATED ZERO DEGREE CROSS SECTION vs INCIDENT PHOTON ENERGY
$S \frac{d\sigma}{d\Omega_{CM}}$ (μ BARN – GeV^2 / STER)
30
20
10
0
5
10
15
K (GeV)
885A1

FIG. 9

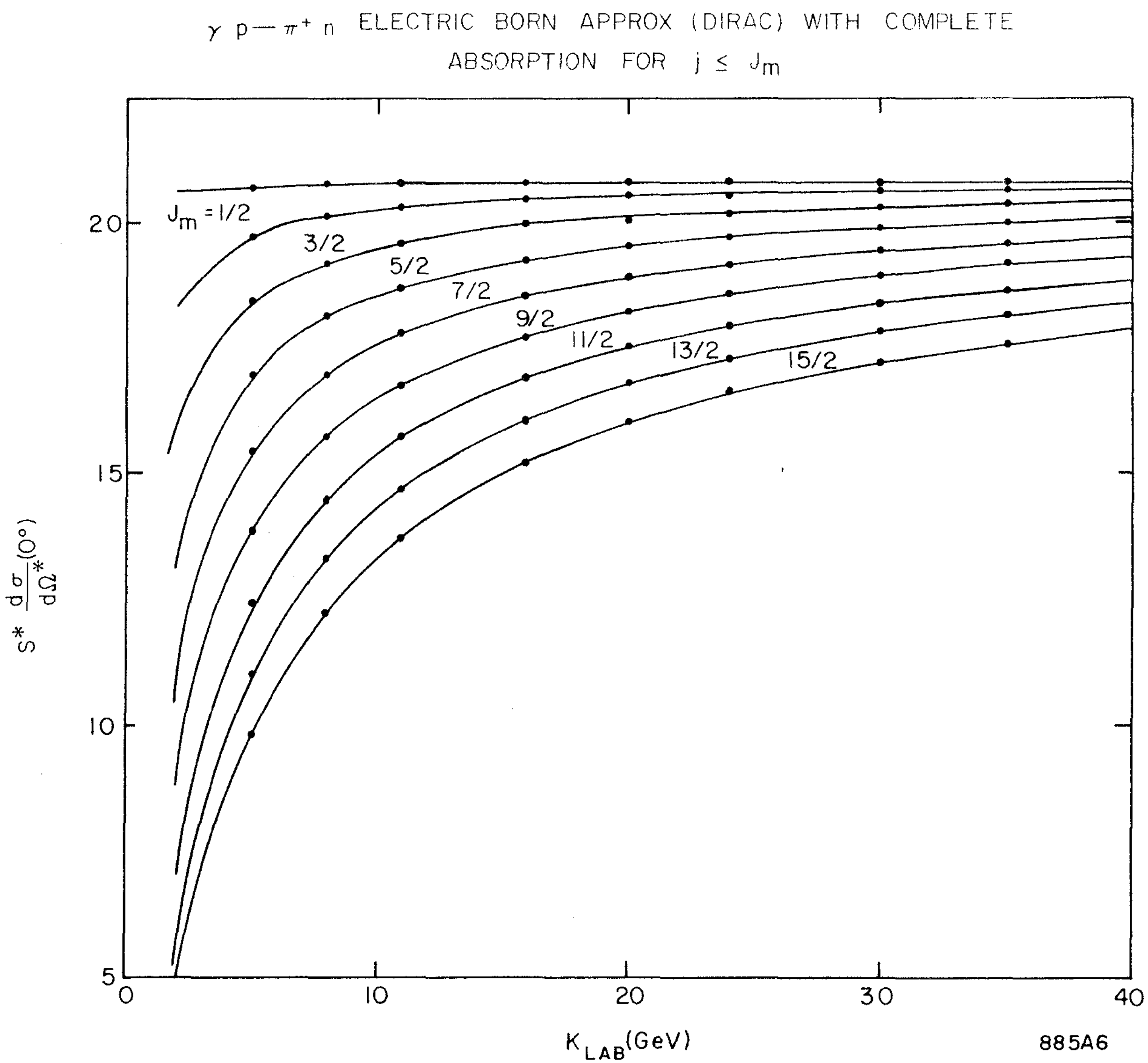

$\gamma\, p \rightarrow \pi^+ n$ ELECTRIC BORN APPROX (DIRAC) WITH COMPLETE
ABSORPTION FOR $j \leq J_m$
$J_m = 1/2$
3/2
5/2
7/2
9/2
11/2
13/2
15/2
20
15
10
5
0
10
20
30
40
$s^* \frac{d\sigma}{d\Omega^*}(0°)$
K_{LAB}(GeV)
885A6

FIG.10

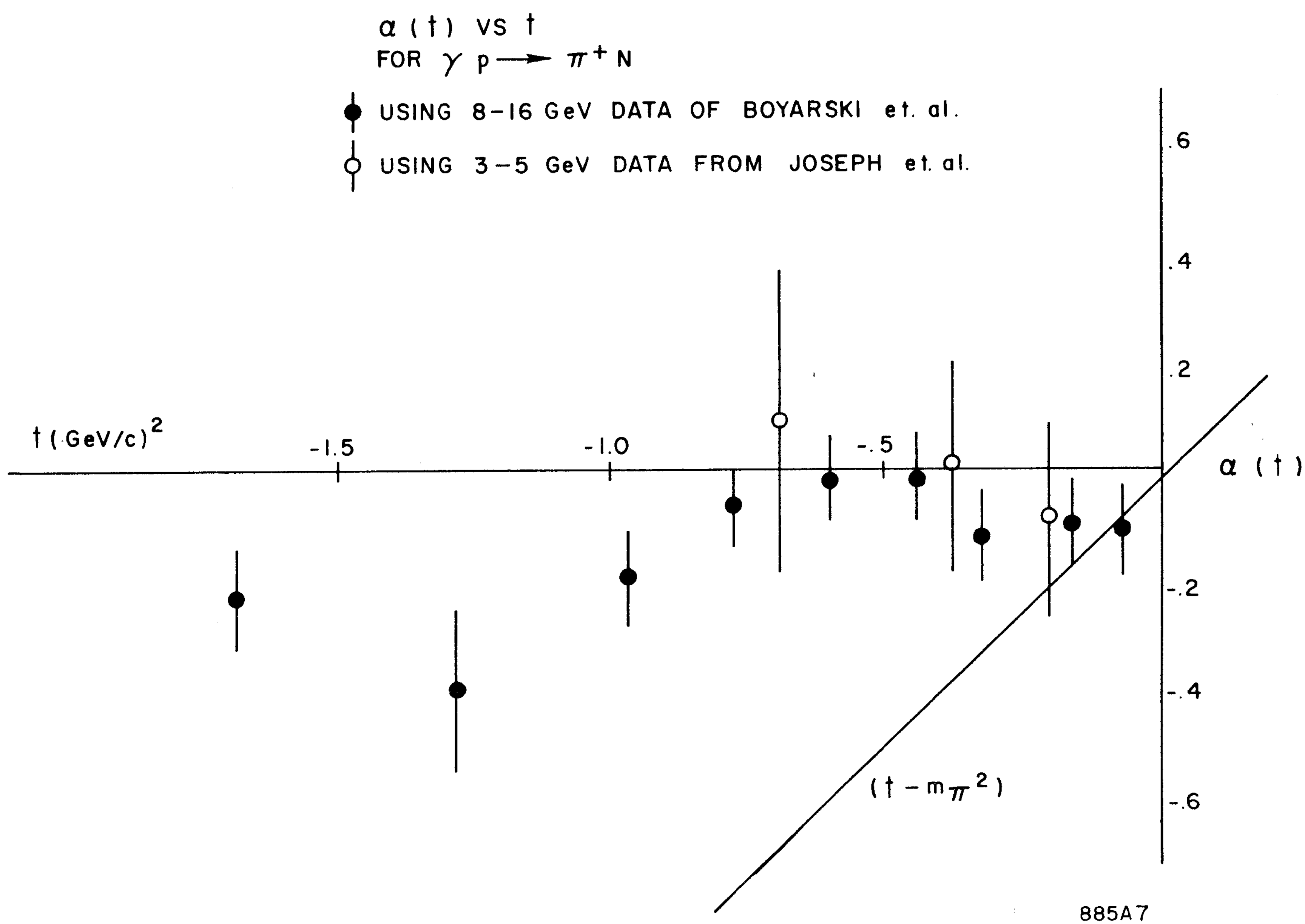

α (t) VS t
FOR γ p ⟶ π⁺ N
USING 8–16 GeV DATA OF BOYARSKI et. al.
USING 3–5 GeV DATA FROM JOSEPH et. al.
t (GeV/c)²
-1.5
-1.0
-.5
.6
.4
.2
-.2
-.4
-.6
α (t)
(t – mπ²)
885A7

FIG. 11

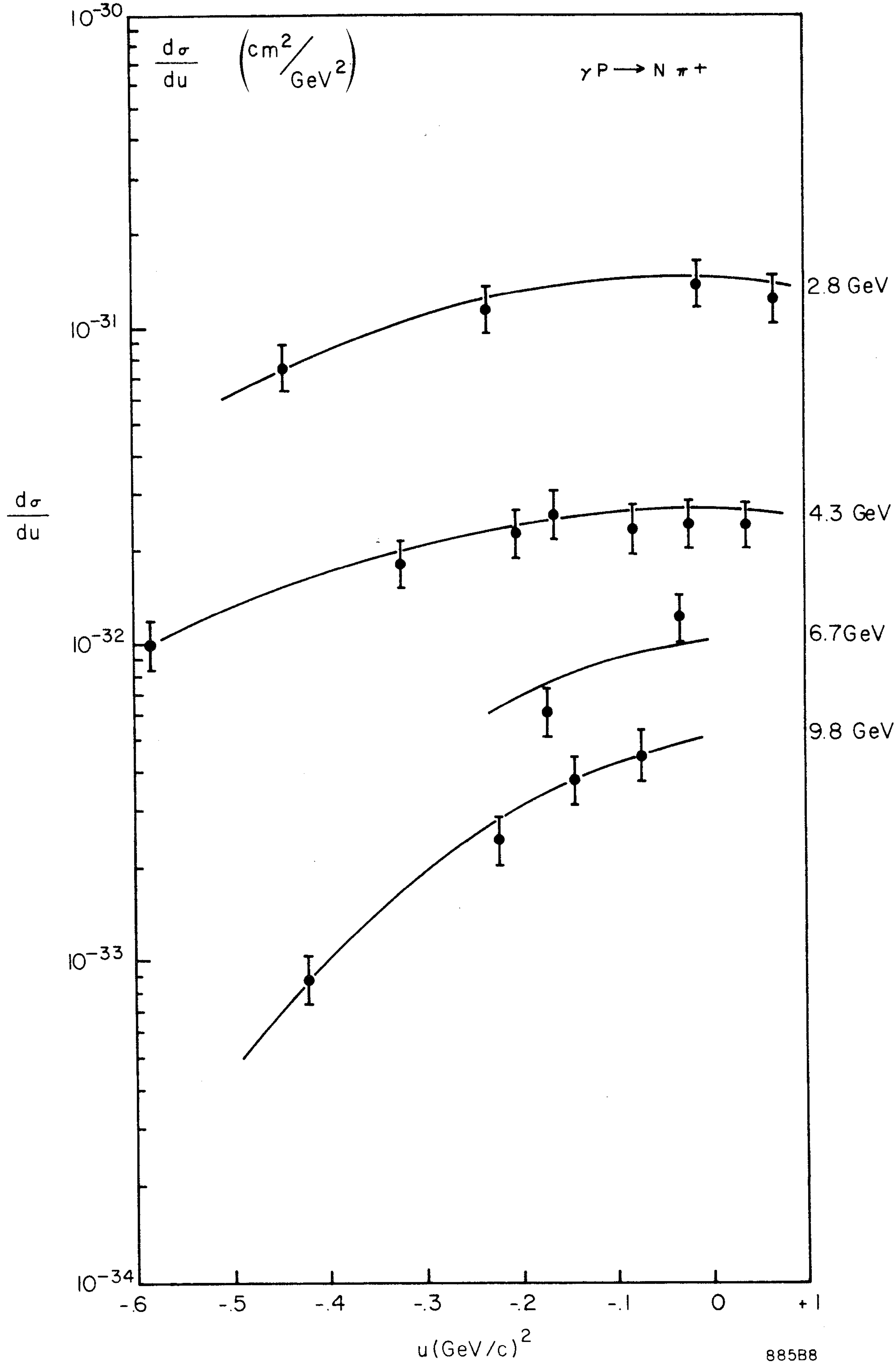

10^{-30}
$\frac{d\sigma}{du}$ $\left(cm^2/GeV^2\right)$
$\gamma P \longrightarrow N\pi+$
10^{-31}
2.8 GeV
$\frac{d\sigma}{du}$
4.3 GeV
6.7GeV
10^{-32}
9.8 GeV
10^{-33}
10^{-34}
-.6
-.5
-.4
-.3
-.2
-.1
0
+1
$u(GeV/c)^2$
885B8

FIG.12

FIG. 9. Pion-proton elastic scattering distributions in the backward peak region at 4 and 8 GeV/c. Results of Ref. 7 are used in addition to the results of this experiment.

■ 4.0 GeV/c Kormanyos *et al.*
△ 4.4 GeV/c ⎫ Brody *et al.*
○ 7.8 GeV/c ⎭
□ 4 GeV/c ⎫ This exp.
● 8 GeV/c ⎭

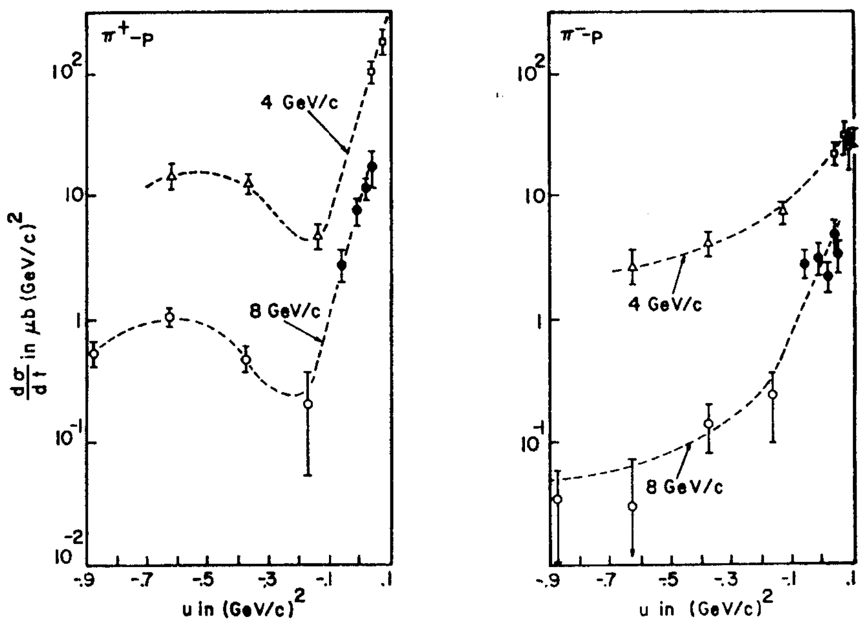

FIG. 13

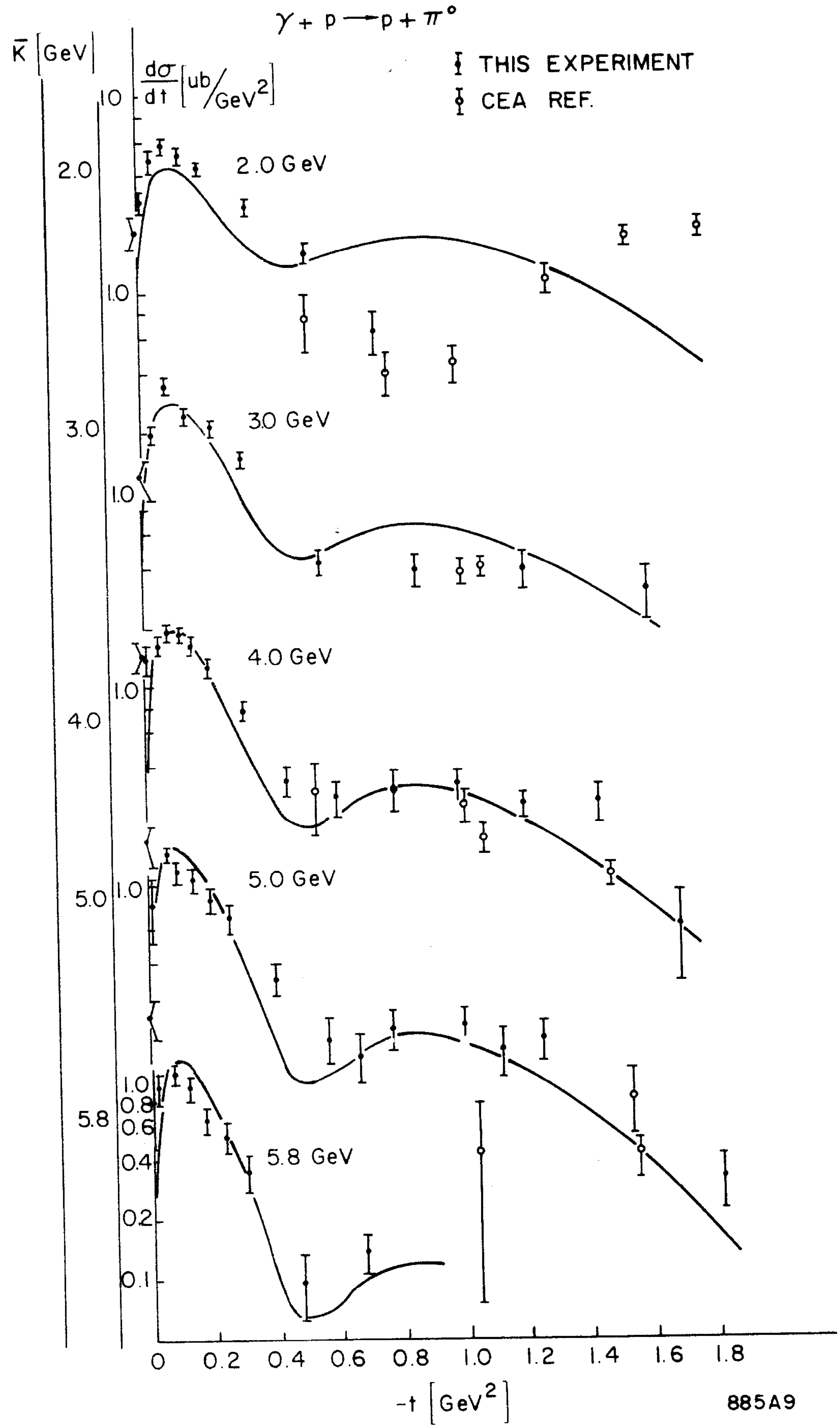

$\gamma + p \rightarrow p + \pi^{\circ}$
THIS EXPERIMENT
CEA REF.
$\bar{K}$ [GeV]
$\frac{d\sigma}{dt}$ [ub/GeV^2]
2.0 GeV
3.0 GeV
4.0 GeV
5.0 GeV
5.8 GeV
$-t$ [GeV^2]
885A9

FIG. 14

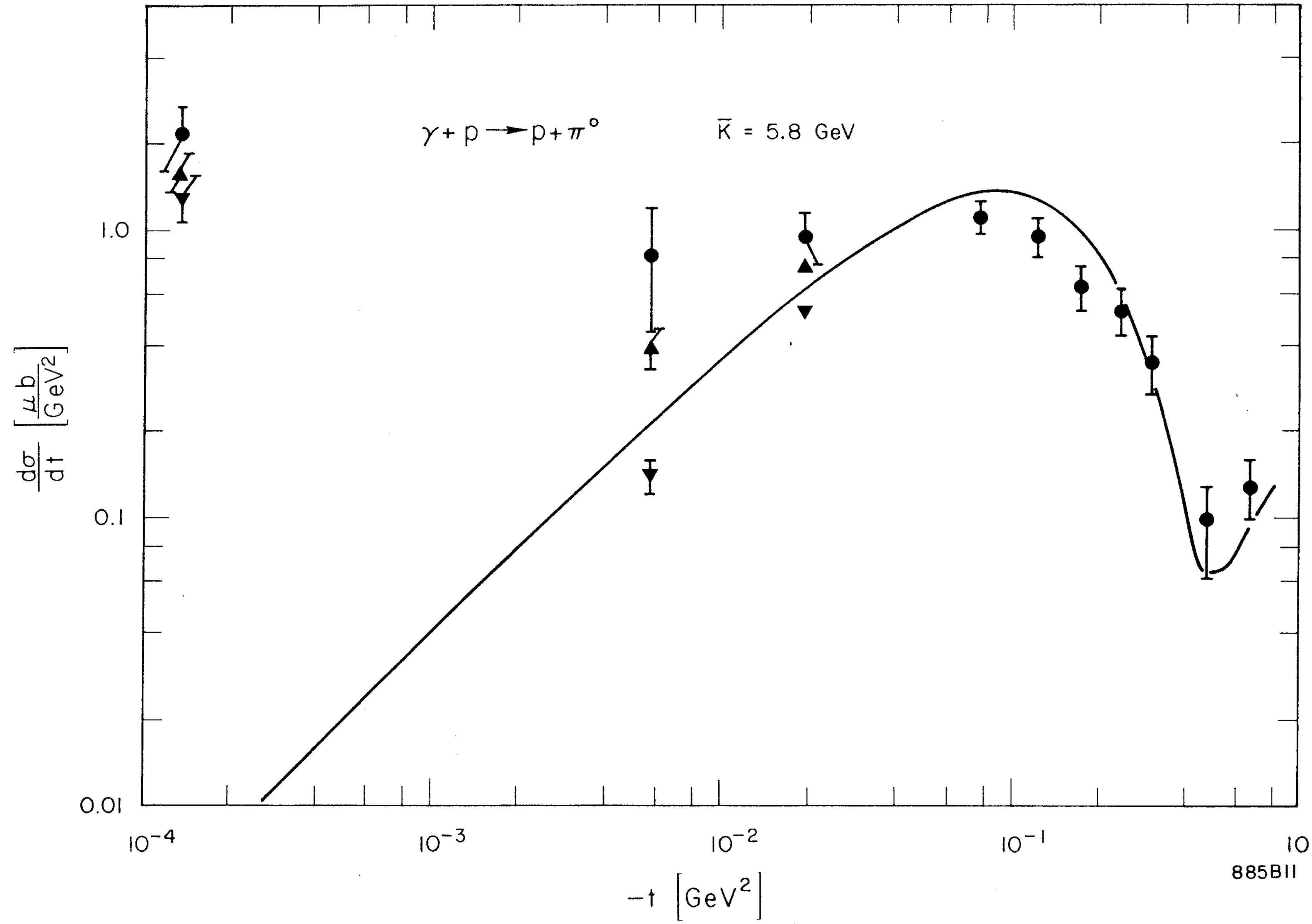

$\gamma + p \longrightarrow p + \pi^0$
$\bar{K}$ = 5.8 GeV
1.0
0.1
0.01
10^{-4}
10^{-3}
10^{-2}
10^{-1}
10
$\frac{d\sigma}{dt}\left[\frac{\mu b}{GeV^2}\right]$
$-t\ [GeV^2]$
885B11

FIG. 15

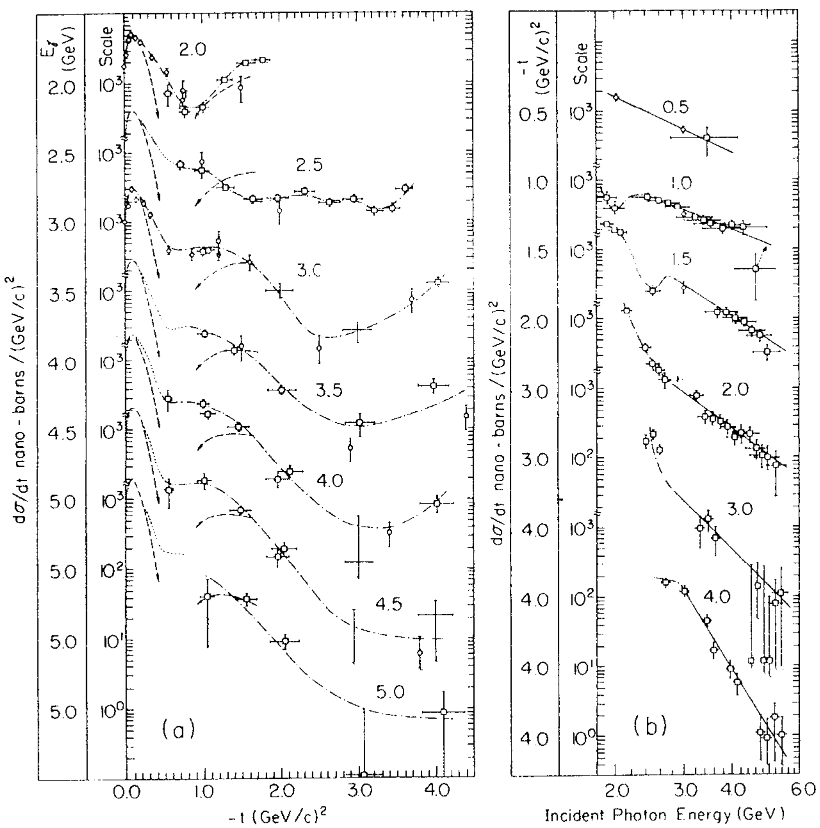

FIG. 1. (a) $d\sigma/dt$ as a function of $-t$ for several incident photon energies: squares, this experiment; circles, earlier Massachusetts Institute of Technology data (Refs. 1 and 2); diamonds, Bonn group (Ref. 4); crosses, this experiment, where the plotted data points are interpolations of data at nearby energies. The interpolation distance for these points was typically ±0.100 GeV. The curves in this figure are described in the text. (b) $d\sigma/dt$ as a function of E_γ for several values of $|t|$. The symbols used to represent different types of data points are the same as for (a). The curves through the data points are described in the text.

FIG. 16

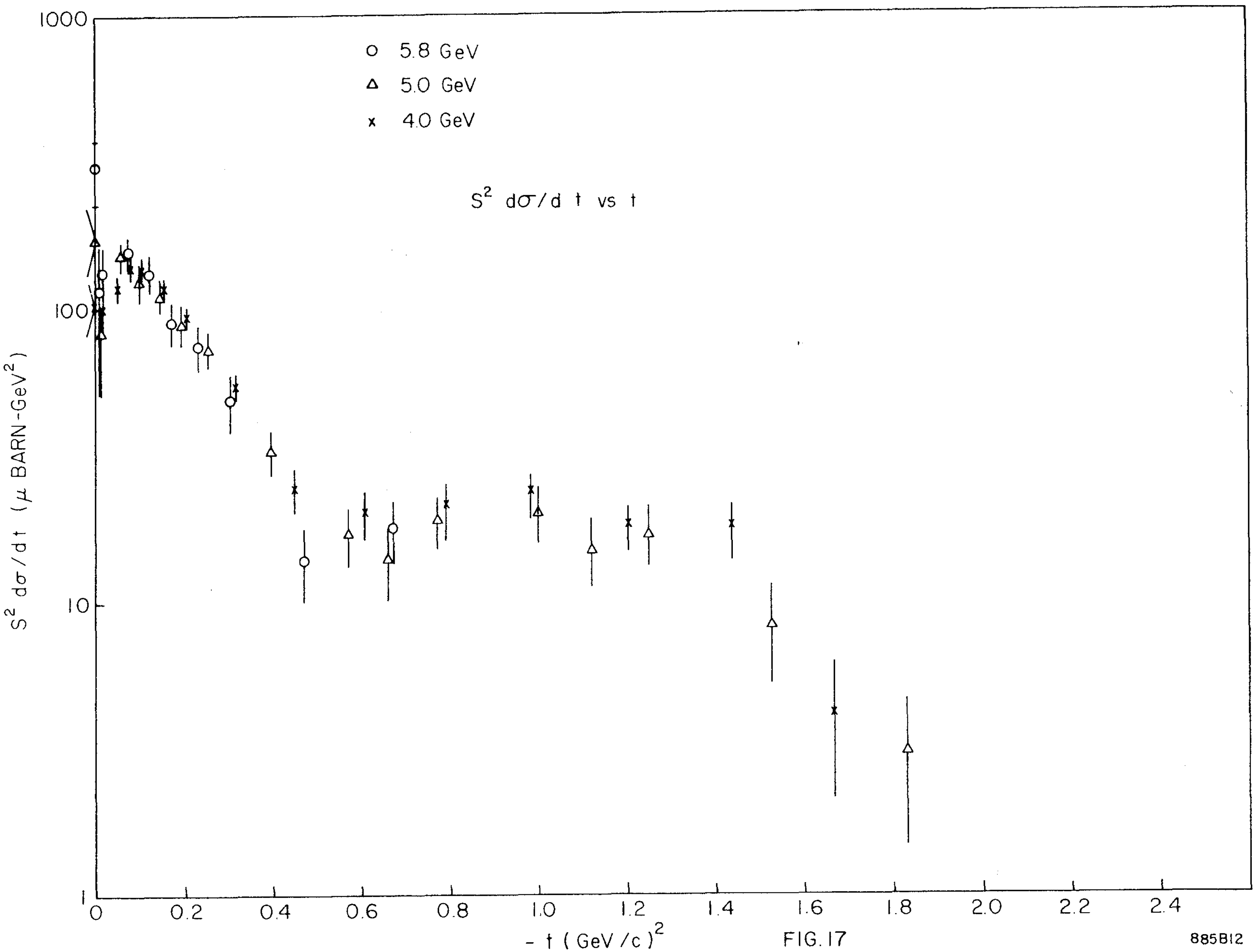

FIG. 17

885B12

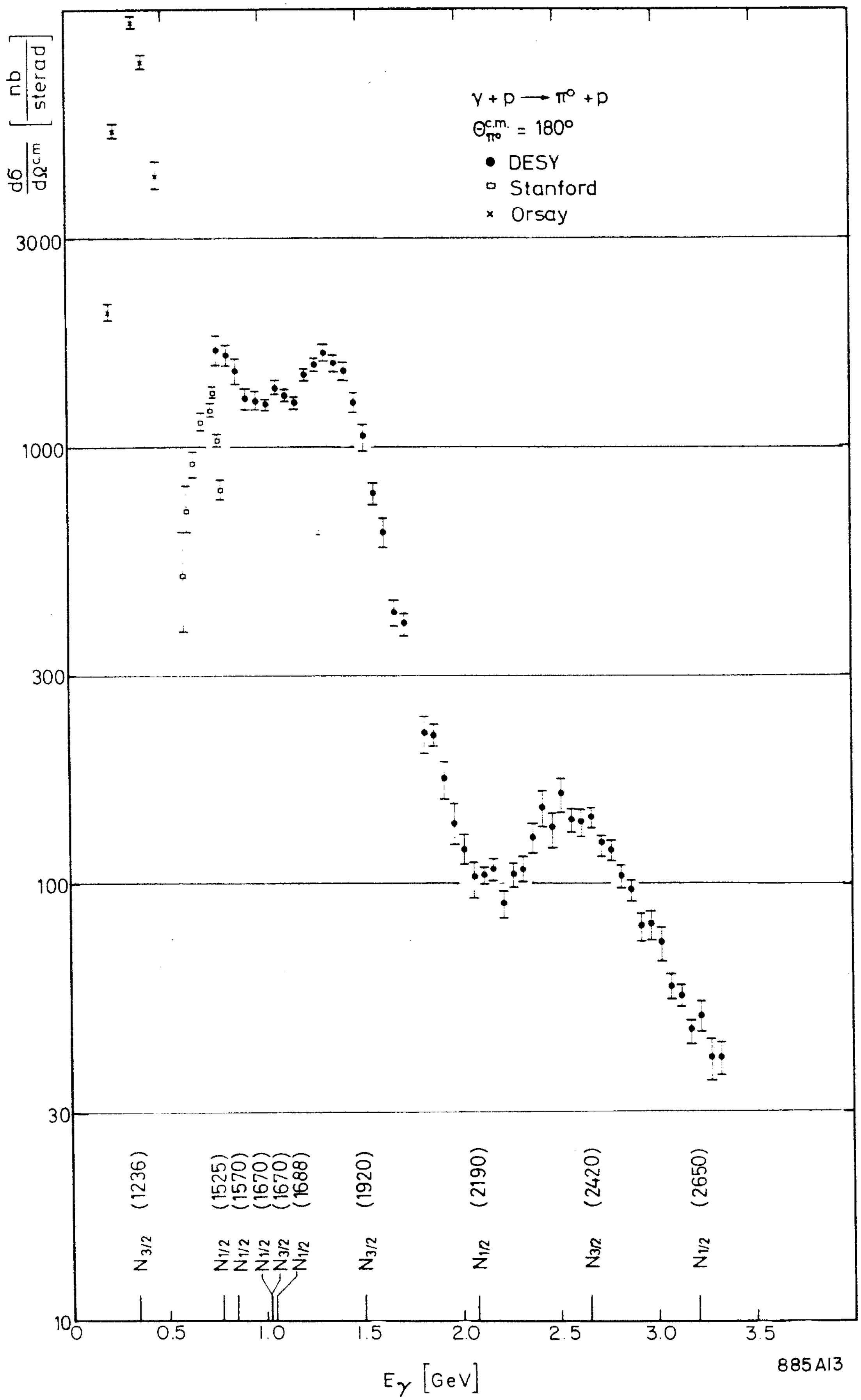

$\gamma + p \longrightarrow \pi^0 + p$
$\Theta_{\pi^0}^{c.m.} = 180°$
DESY
Stanford
Orsay
$\frac{d\sigma}{d\Omega^{c.m.}}\left[\frac{nb}{sterad}\right]$
3000
1000
300
100
30
10
0
0.5
1.0
1.5
2.0
2.5
3.0
3.5
$N_{3/2}$ (1236)
$N_{1/2}$ (1525)
$N_{1/2}$ (1570)
$N_{1/2}$ (1670)
$N_{3/2}$ (1670)
$N_{1/2}$ (1688)
$N_{3/2}$ (1920)
$N_{1/2}$ (2190)
$N_{3/2}$ (2420)
$N_{1/2}$ (2650)
E_γ [GeV]
885A13

FIG. 18

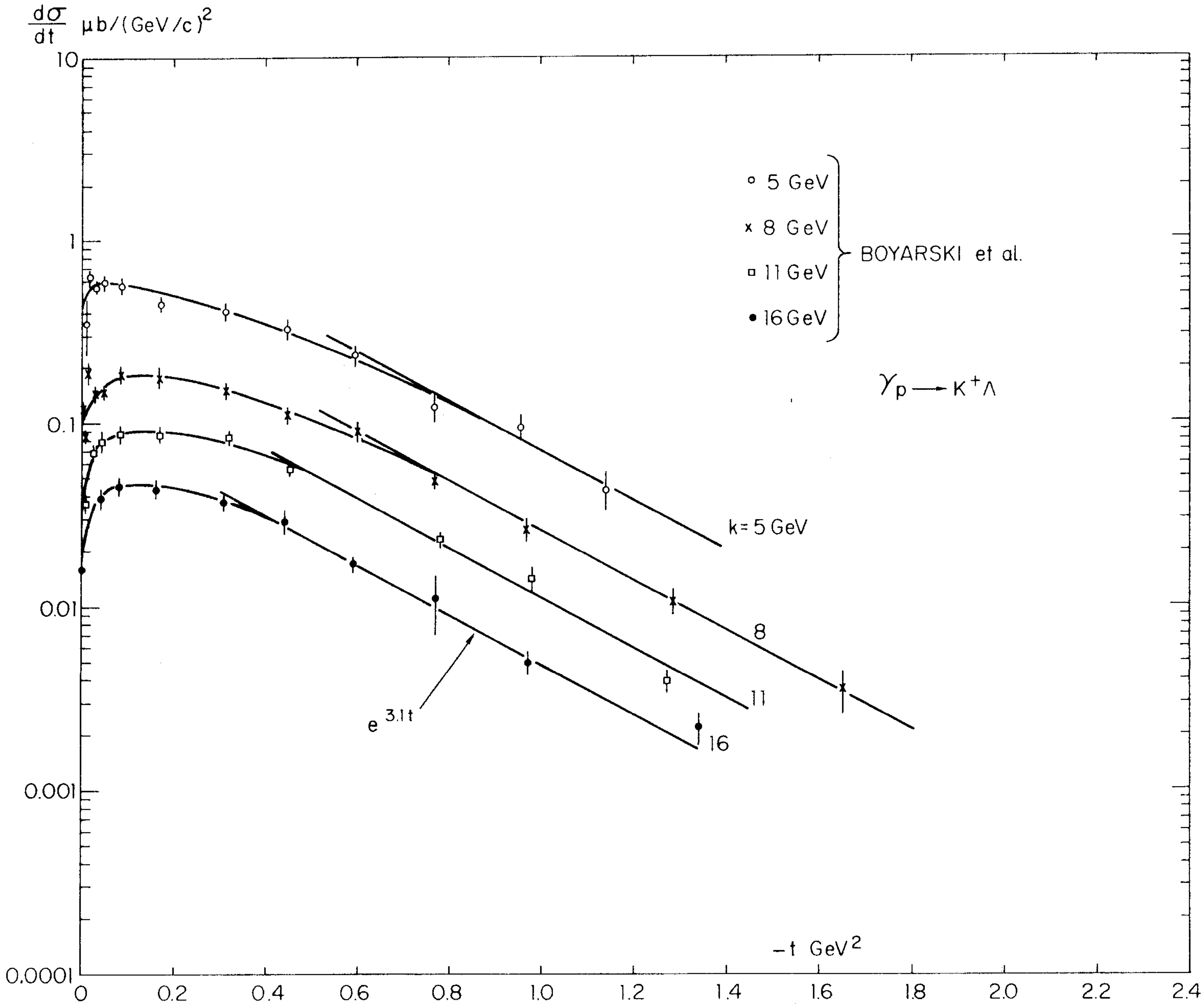

$\frac{d\sigma}{dt}$ $\mu b/(GeV/c)^2$
10
1
0.1
0.01
0.001
0.0001
0
0.2
0.4
0.6
0.8
1.0
1.2
1.4
1.6
1.8
2.0
2.2
2.4
∘ 5 GeV
× 8 GeV
▫ 11 GeV
• 16 GeV
BOYARSKI et al.
$\gamma p \longrightarrow K^+\Lambda$
k = 5 GeV
8
11
16
$e^{3.1t}$
$-t$ GeV^2

FIG. 19

877C6

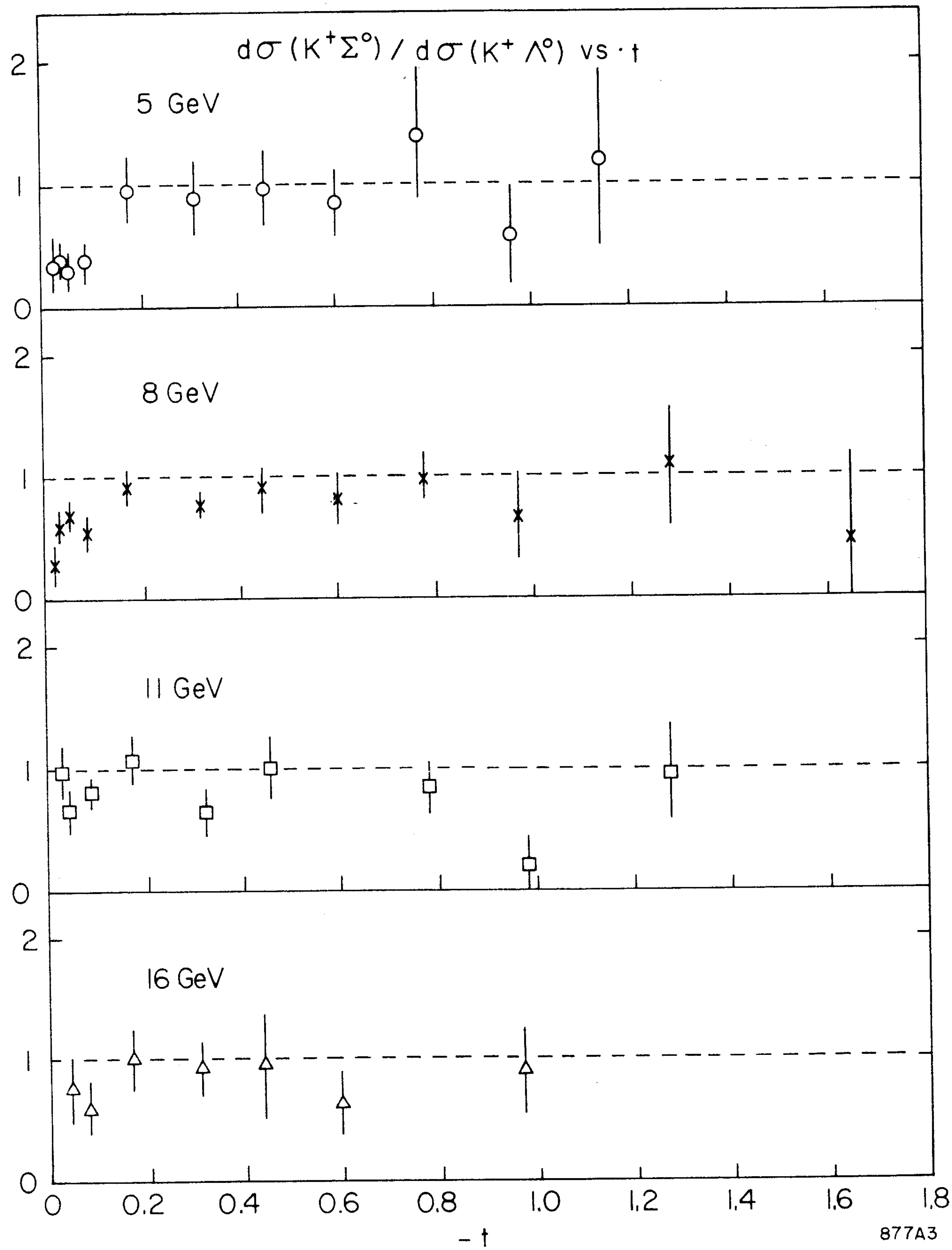
dσ (K⁺Σ°) / dσ (K⁺ Λ°) vs · t
5 GeV
8 GeV
11 GeV
16 GeV
0
1
2
0
0.2
0.4
0.6
0.8
1.0
1.2
1.4
1.6
1.8
- t
877A3

FIG. 20

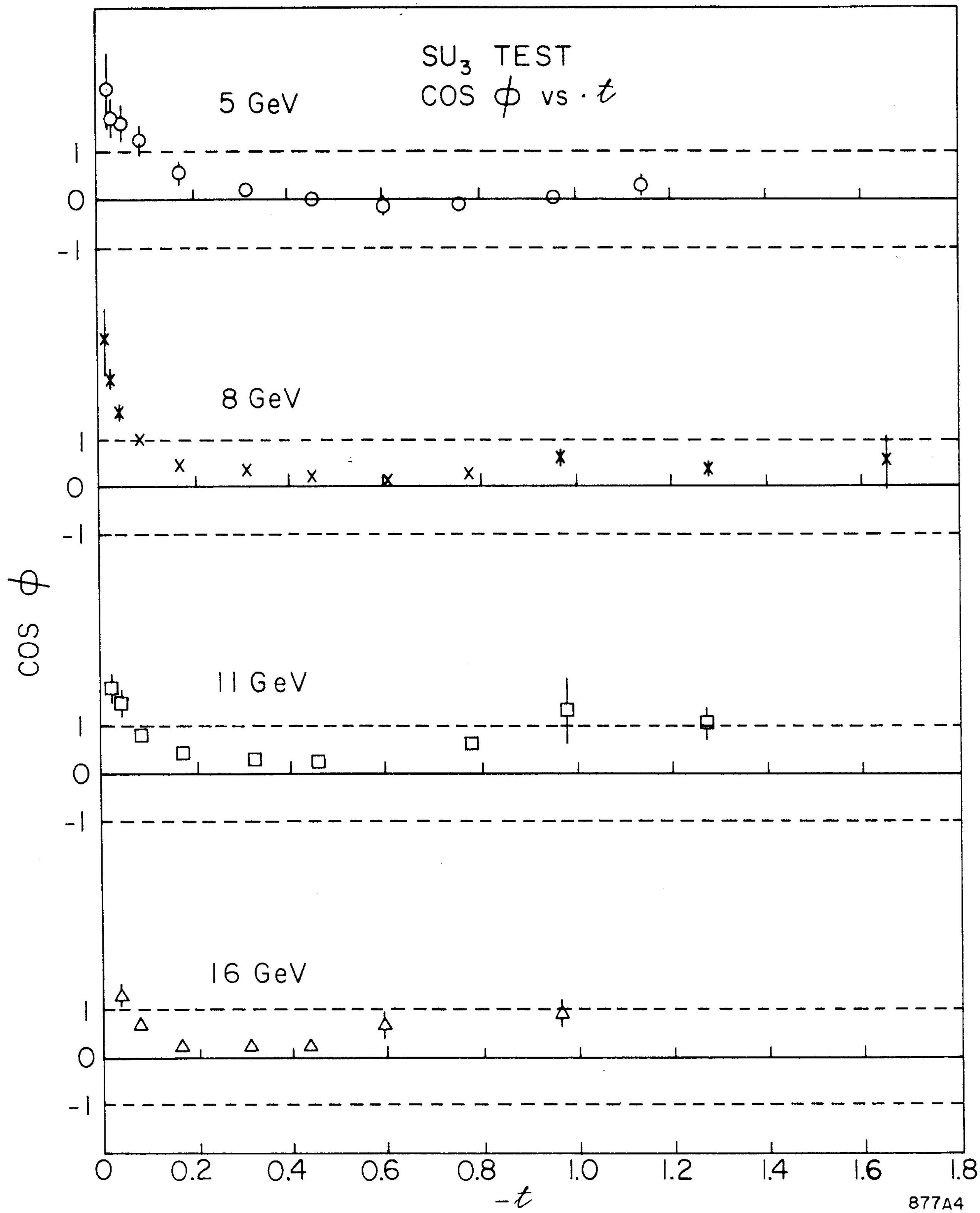

SU3 TEST
COS φ vs · t
5 GeV
8 GeV
11 GeV
16 GeV
COS φ
1
0
-1
0
0.2
0.4
0.6
0.8
1.0
1.2
1.4
1.6
1.8
-t
877A4

FIG. 21

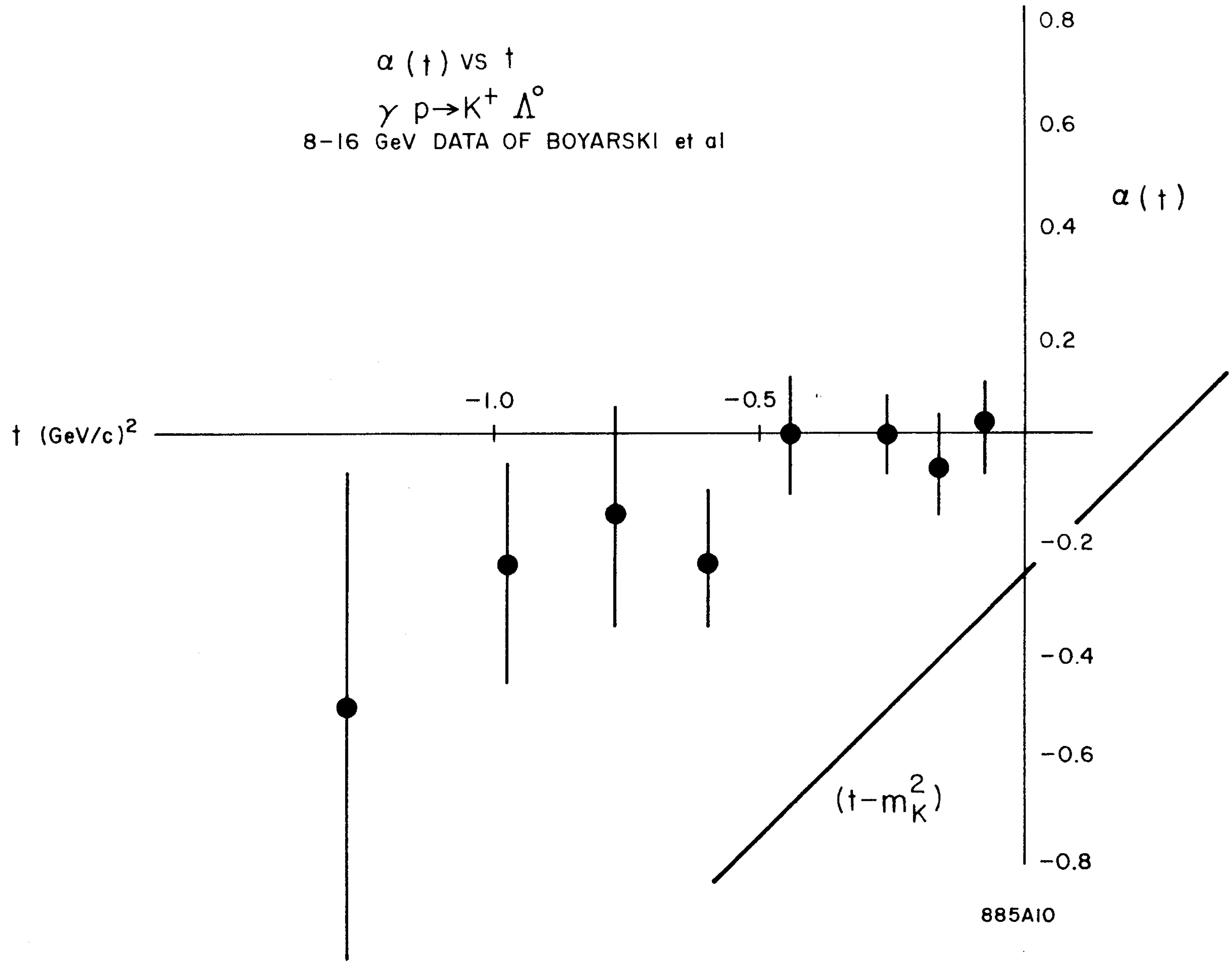

α (t) vs t
γ p→K+ Λ°
8-16 GeV DATA OF BOYARSKI et al
t (GeV/c)²
-1.0
-0.5
0.8
0.6
0.4
0.2
-0.2
-0.4
-0.6
-0.8
α (t)
(t-m²K)
885A10

FIG. 22

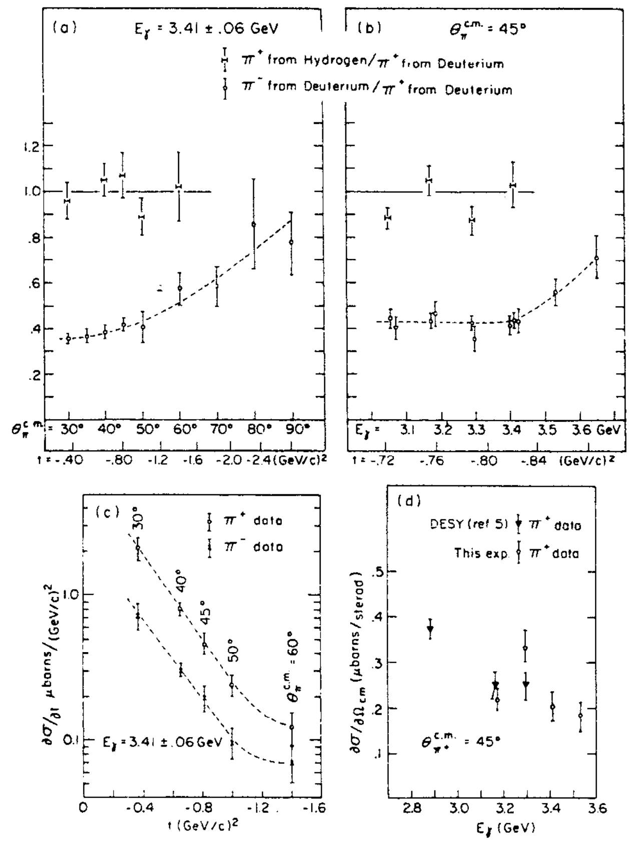

FIG. 2. (a), (b) π^-/π^+ ratio and (π^+ from H_2)/(π^+ from D_2) ratio as functions of $\theta_\pi{}^{c.m.}$ (a) and E_γ (b). (c) $d\sigma/dt$ and (d) $d\sigma/d\Omega^{c.m.}$ for single-pion photoproduction; the π^+ cross sections include both hydrogen and deuterium data from Reactions (ii) and (iii); for reasons of counting statistics, the π^- cross sections in (c) are obtained using the π^+ cross sections and the π^-/π^+ ratio.

FIG. 23